

AD 737241

EVALUATION OF VARIOUS  
THEORETICAL MODELS FOR  
UNDERWATER EXPLOSION

APRIL 71

AN EVALUATION OF VARIOUS THEORETICAL MODELS  
FOR UNDERWATER EXPLOSION BUBBLE PULSATION

by

John W. Pritchett

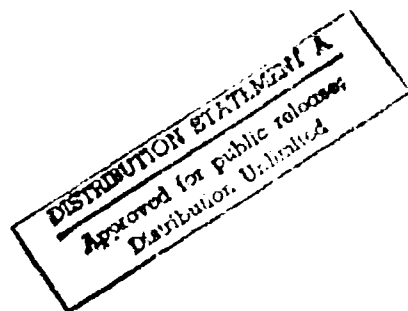
IRA-TR-2-71

15 April 1971

The views and conclusions contained in this document are those of the author and should not be interpreted as necessarily representing the official policies, either expressed or implied, of the Advanced Research Projects Agency or the United States Government.

This research was sponsored by the Advanced Research Projects Agency of the Department of Defense and was monitored by the Office of Naval Research under Contract No. N00014-70-C-0260.

INFORMATION RESEARCH ASSOCIATES  
125 UNIVERSITY AVENUE  
BERKELEY MARINA  
BERKELEY, CALIFORNIA 94710  
PHONE: (415) 843-1379



## ABSTRACT

A number of theoretical calculations of the motion of a spherical underwater explosion bubble oscillating in an incompressible homogeneous unbounded inviscid fluid are presented, using various "models" for the behavior of the bubble interior. The purpose of this study was to find an adequate representation for use in axisymmetric calculations of underwater nuclear explosion effects in which the bubble may become non-spherical due to the effects of gravity and/or nearby boundaries. The cases considered include (1) neglecting the bubble atmosphere altogether; that is, treating the bubble as an evacuated cavity, (2) treating the bubble interior as an adiabatic homogeneous ideal gas, but ignoring the inertial effects of the gas, (3) including the gas inertial effects in the previous case, (4) replacing the ideal gas behavior in case 2 with equation-of-state data for real steam, and (5) reverting to an ideal gas for simplicity, dropping the assumption of bubble homogeneity; that is, the gas dynamics of the bubble interior were followed by explicit numerical integration of Euler's equations using a Lagrangian finite-difference computer code. Except for case 1, the results were found to be virtually identical and in good agreement both with experimental measurements and with calculations performed by other investigators which take into consideration the compressibility of the water outside the bubble.

# TABLE OF CONTENTS

	<u>page</u>
I. INTRODUCTION	7
II. FORMATION OF THE EXPLOSION BUBBLE	11
III. DESCRIPTION OF BUBBLE PULSATION	17
IV. TWO-DIMENSIONAL EFFECTS	21
V. SOLUTIONS NEGLECTING THE BUBBLE ATMOSPHERE	27
VI. THE IDEAL GAS MODEL	39
VII. REAL-STEAM EFFECTS	55
VIII. BUBBLE ATMOSPHERE DYNAMICS	59
IX. COMPARISONS WITH OTHER RESULTS	65
X. ACKNOWLEDGEMENTS	81
XI. REFERENCES	83
APPENDIX A - SYMBOLS AND ABBREVIATIONS	87
APPENDIX B - INITIAL DISTRIBUTION	91
APPENDIX C - D.D. FORM 1473	95

# FIGURES

	<u>page</u>
1. TNT Charge Radius and Reaction Time vs. Yield	13
2. Early Shockwave Energy Dissipation for a One-Kiloton TNT Charge	14
3. The Effects of Bubble Energy Loss - The Non-Migrating Case	20
4. The Gasless Model - Square of the Mach Number Vs. Bubble Radius for a One-Kiloton Explosion	32
5. The Gasless Model - Square of the Mach Number Vs. Time for a One-Kiloton Explosion	33
6. The Gasless Model - The Dimensionless Bubble Radius-Time Relation	36
7. The Gasless Model - The Bubble Energy Balance	36
8. The Ideal Gas Model - The Dimensionless Radius-Time Relation for $\gamma = 4/3$ and Relative Intensity $\zeta = 3000$	46
9. The Ideal Gas Model - The Bubble Energy Balance for $\gamma = 4/3$ and Relative Intensity $\zeta = 3000$	46
10. The Ideal Gas Model - The Dimensionless Maximum Bubble Radius $A$ as a Function of $\gamma$ and $\zeta$	48
11. The Ideal Gas Model - The Dimensionless Oscillation Period $\sigma\tau$ as a Function of $\gamma$ and $\zeta$	49
12. The Ideal Gas Model - The Dimensionless Characteristic Velocity $\mu$ as a Function of $\gamma$ and $\zeta$	50
13. The Ideal Gas Model - The Shape Factor $B$ as a Function of $\gamma$ and $\zeta$	51
14. The Ideal Gas Model - The Effect of Gas Inertia on the Characteristic Velocity	52
15. The Ideal Gas Model - The Effect of Gas Inertia on the Shape Factor $B$	53
16. Deviation of the Ideal Gas Model Results from the Real-Steam Calculation	57
17. Comparison of the "Average" Experimental Dimensionless Oscillation Period for TNT with Ideal Gas Model Results	67
18. Comparison of the Dimensionless WIGWAM Bubble Period with Ideal Gas Model Results	69
19. Comparison of the "Average" Experimental Dimensionless Maximum Bubble Radius for TNT with Ideal Gas Model Results	71

20. Pressure Distribution in the Water for Various Times After Burst	72
21. Critical Ambient Hydrostatic Pressure Below Which Bubble Surface May Boil at the Bubble Maximum as a Function of Water Temperature	74
22. Comparison of the Dimensionless Maximum Bubble Radii ( $\Lambda$ ) Predicted by Compressible-Water Calculations with Ideal Gas-Incompressible Water Results	77
23. Comparison of the Dimensionless Characteristic Velocities ( $\mu$ ) Predicted by Compressible-Water Calculations with Ideal Gas-Incompressible Water Results	78

UNCLASSIFIED

Security Classification

## DOCUMENT CONTROL DATA - R &amp; D

(Security classification of title, body of abstract and indexing annotation must be entered when the overall report is classified)

1. ORIGINATOR'S NAME (Corporate author)		2a. REPORT SECURITY CLASSIFICATION	
Information Research Associates, Inc. 125 University Avenue, Berkeley Marina Berkeley, California 94710		UNCLASSIFIED	
3. REPORT TITLE		2b. GROUP	
AN EVALUATION OF VARIOUS THEORETICAL MODELS FOR UNDERWATER EXPLOSION BUBBLE PULSATION			
4. DESCRIPTIVE NOTES (Type of report and inclusive dates)			
Interim			
5. AUTHOR(S) (First name, middle initial, last name)			
John W. Pritchett			
6. REPORT DATE	7a. TOTAL NO. OF PAGES	7b. NO. OF REFS	
15 April 1971	89	25	
8. CONTRACT OR GRANT NO.	9a. ORIGINATOR'S REPORT NUMBER(S)		
N00014-70-C-0260 ARO-ECY NO ARPA Order No. 1593	IRA-TR-2-71		
9b. OTHER REPORT NO(S) (Any other numbers that may be associated with this report)			
10. DISTRIBUTION STATEMENT			
Approved for public release: distribution unlimited.			
11. SUPPLEMENTARY NOTES		12. SPONSORING MILITARY ACTIVITY	
		The Advanced Research Projects Agency	
13. ABSTRACT			
<p>A number of theoretical calculations of the motion of a spherical underwater explosion bubble oscillating in an incompressible homogeneous unbounded inviscid fluid are presented, using various "models" for the behavior of the bubble interior. The purpose of this study was to find an adequate representation for use in axisymmetric calculations of underwater nuclear explosion effects in which the bubble may become non-spherical due to the effects of gravity and/or nearby boundaries. The cases considered include (1) neglecting the bubble atmosphere altogether; that is, treating the bubble as an evacuated cavity, (2) treating the bubble interior as an adiabatic homogeneous ideal gas, but ignoring the inertial effects of the gas, (3) including the gas inertial effects in the previous case, (4) replacing the ideal gas behavior in case 2 with equation-of-state data for real steam, and (5) reverting to an ideal gas for simplicity, dropping the assumption of bubble homogeneity; that is, the gas dynamics of the bubble interior were followed by explicit numerical integration of Euler's equations using a Lagrangian finite-difference computer code. Except for case 1, the results were found to be virtually identical and in good agreement both with experimental measurements and with calculations performed by other investigators which take into consideration the compressibility of the water outside the bubble.</p>			

NOV 1973

REPLACES DD FORM 1073, 1 JAN 69, WHICH IS OBSOLETE FOR ARMY USE.

UNCLASSIFIED

Security Classification

UNCLASSIFIED

UNCLASSIFIED		UNCLASSIFIED		UNCLASSIFIED		UNCLASSIFIED	
UNCLASSIFIED		UNCLASSIFIED		UNCLASSIFIED		UNCLASSIFIED	
Underwater explosions							
Explosion bubbles							
Incompressible flow							
Weapons effects							

## I. INTRODUCTION

Underwater explosion effects have been the subject of extensive study for many years, particularly since the beginning of World War II. Most of the early research concerned the characterization of the shock wave caused by the explosion and its interaction with the water surface, the sea bottom, and (especially) targets such as the hulls of ships and submarines. The effects of the shockwave may be felt at very large distances and occur on a very short time-scale due to the high speed of sound in water. The late-time effects of the explosion (that is, the pulsation and migration of the residual "bubble" of gas, its eruption from the surface, the resulting water waves, and similar phenomena) received much less attention. This was, of course, only natural, since the military importance of these phenomena is usually relatively marginal for conventional underwater ordnance.

When nuclear (and later, thermonuclear) explosives were developed, however, the available energy release of underwater weapons increased by several orders of magnitude. The secondary late-time mass-motion effects consequently acquired new significance, and therefore, in recent years, these effects have been much more extensively studied than previously. One of the effects of underwater nuclear explosions which immediately comes to mind is that of the dispersal of the radioactive nuclear debris; the transport of this residue from the point of burst to the above-surface environment is governed by the late-time motion of the steam bubble produced by the explosion. Another effect of military significance, particularly for large explosions, is the generation of large water surface waves which could pose a serious threat to naval units or could even inundate a nearby coastline.

The mass-motion effects of an underwater explosion, as compared to those of the shockwave, are fairly slow and distant.

After the emission of the shock, the hot gases formed by the explosion expand; if the explosion is shallow enough, this gas bubble may erupt from the water surface during the first expansion. Otherwise, the bubble will expand to a maximum size, then contract to a minimum size, re-expand, and continue to pulsate with diminishing amplitude. At the same time, the bubble will migrate upward toward the surface due to its buoyancy. For nuclear explosions, this bubble oscillation-migration phase occurs on a time scale of several seconds as compared to milliseconds for shock wave effects, and therefore the motion is virtually always subsonic. The eruption of the bubble from the surface will hurl large masses of water aloft, releasing the contained fission products, generating large surface waves that thereafter propagate away from surface zero, and setting into motion other familiar late-time explosion effects (the residual upwelling along the explosion axis, the turbulent diffusion of the radioactive surface "pool", and so on).

Since the bubble pulsation, migration, plume eruption and subsequent events are fairly slow-motion phenomena, the water motion may be adequately treated as incompressible flow. Even so, however, the problem is in general at least two-dimensional (that is, axisymmetric) and time dependent, and involves free surfaces. Therefore, the theoretical treatment of the motion is quite complicated, and consequently most of the information available today has been collected by experimental means. Recently, however, the development of modern high-speed third generation digital computers has rendered purely theoretical calculations of axisymmetric bubble motion feasible.

The MACYL6 hydrodynamic code (Pritchett, 1970a) was designed specifically to compute the water motion around a pulsating, migrating explosion bubble, including late-time plume eruption and subsequent phenomena, by brute-force numerical integration using finite-difference techniques of the fundamental governing equations of hydrodynamics in axisymmetric geometry.

The computer program has been used successfully in the past to compute the late-time flow after various underwater nuclear explosions, and agreement with experimental results (where available) has been good (see, for example, Pritchett and Pestaner, 1969; Pritchett, 1970b; Pritchett, 1971). It is now being put to use to study the formation of surface waves by deep underwater nuclear explosions.

In order to use the MACYL6 code to describe an underwater explosion, however, the boundary conditions must be specified; air pressure is, of course, imposed at the air-water interface and remains constant with time. At the bubble-water interface, a pressure must also be prescribed in some realistic manner. That is, the MACYL6 code computes the flow in the water surrounding the bubble, but the gas dynamics within the bubble itself must be "modelled" in some approximate fashion so as to supply the required boundary pressure. In the calculations published to date, the bubble pressure was assumed to be a function of bubble volume, and represents the equilibrium pressure of an ideal gas undergoing adiabatic expansion and recompression. In this report, various "models" of the explosion bubble interior are examined to determine the extent to which various effects alter the overall behavior, with the objective of evaluating the error committed by adopting one or another of these models for use in MACYL6 calculations. In all cases, the water outside the bubble is considered incompressible as in the MACYL6 code, and the bubble is assumed to remain spherical throughout its motion. A bubble-interior "model" which adequately describes a spherical explosion bubble should describe the more general case equally well.

Some of the explosion bubble models which will be discussed in the subsequent sections have been investigated in the past by other workers in the field. The "gasless" case discussed in section V has been studied by many authors, among them Lamb (1932), Willis (1941) and Cole (1948). The ideal gas model

of section VI has been treated by Friedman (1947) and by Snay and Christian (1952) at some length. Many of these early results were, however, limited in precision since the solutions necessarily involve extensive numerical integrations. Therefore, the results presented herein were all computed quite accurately using very finely-resolved numerical integration procedures on a CDC-6600 computer. Furthermore, the results for all cases are presented in a consistent way to facilitate comparison among the various models of bubble behavior.

In the final section, the results of these calculations are compared both with experimental measurements and with a few compressible calculations of the water motion carried out by other investigators; in general, the incompressible-water approximation is seen to be good. Before proceeding to the development of the various bubble models, however, the general phenomenology of underwater explosions will be qualitatively described.

## II. FORMATION OF THE EXPLOSION BUBBLE

The detonation of a submerged explosive sets into motion a complex sequence of events of which the character depends on the nature of the explosive, the energy released, the depth of burst, and other environmental parameters. Nuclear explosions are of primary interest in this study, but most of the experimental information available concerning underwater explosion effects was gathered using chemical explosives. Therefore, in this discussion, both types of explosions will be described, taking note of the differences in effects.

First, we will consider an uncased spherical charge of conventional high-explosive (such as TNT) initiated at the center. As the detonation front expands through the charge, the solid explosive encompassed undergoes chemical reaction and releases energy to further drive the detonation shock. The detonation wave speed is typically in the range 6000-7000 meters per second for most explosives. Behind the detonation front, the "burned" reaction products will include such materials as CO, CO<sub>2</sub>, H<sub>2</sub>O, NO, CH<sub>4</sub> and H<sub>2</sub> as gases, and C, Pb, and Al<sub>2</sub>O<sub>3</sub> as solids. Ultimately, of course, the detonation wave will reach the charge surface and proceed into the water as a strong hydrodynamic shock wave at which time the chemical reactions will be complete. For a given explosive type and packing density, the total energy released by the explosion will be proportional to the charge mass; that is:

$$Y = \frac{4}{3} \pi R_0^3 \rho_E Q \quad (II-1)$$

where

Y = yield; total explosion energy

R<sub>0</sub> = charge radius

$\rho_E$  = explosive packing density

$Q$  = chemical energy released per unit explosive mass.

Furthermore, the "reaction time" (time required for the detonation process) will depend on the charge size and the detonation wave speed:

$$t_R = \frac{R_0}{C_{det}} = \left[ \frac{3Y}{4\pi\rho_E Q C_{det}^3} \right]^{1/3} \quad (II-2)$$

For TNT, for example, a typical packing density is about 1500 kg/m<sup>3</sup> (that is, a specific gravity of 1.5) and  $Q$  is approximately  $4.2 \times 10^6$  joules/kg. Therefore, a spherical TNT charge with an energy release of one kiloton (defined as  $10^{12}$  calories or about  $4.2 \times 10^{12}$  joules) would be about 10.9 meters in diameter, and the total reaction time would be slightly less than one millisecond (see Figure 1).

Initially, the shock propagated into the water contains about half the explosion energy; the remainder resides as both kinetic energy associated with the expansion of the gaseous "bubble" of reaction products, and as internal energy (heat) within the explosion products themselves. This shock travels away rapidly, declining in strength. Near the original charge position, the highly non-linear behavior of the shock causes energy dissipation as heat to the water. Once the shock is about 10 or 15 charge radii from the origin, however, this dissipation process is largely complete; the shock thereafter continues to travel away carrying with it about one-fourth of the original explosion energy (see Figure 2). The time interval from the moment of explosion to the end of this "dissipation" phase (defined for our purposes as the moment when the shock has propagated 10 charge radii) is still fairly short, but is about 25 times greater than the "reaction time".

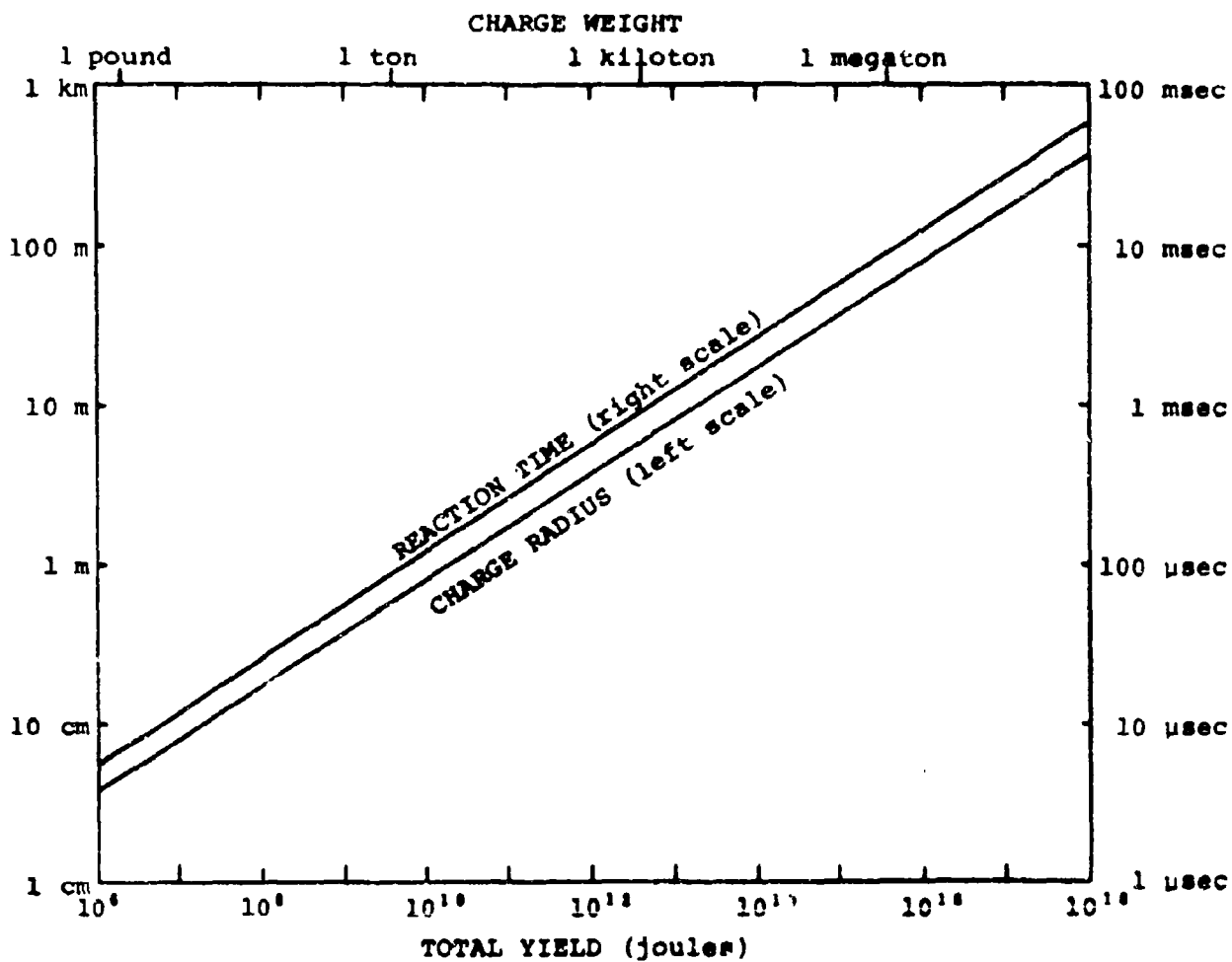


FIGURE 1: TNT CHARGE RADIUS AND REACTION TIME VS. YIELD

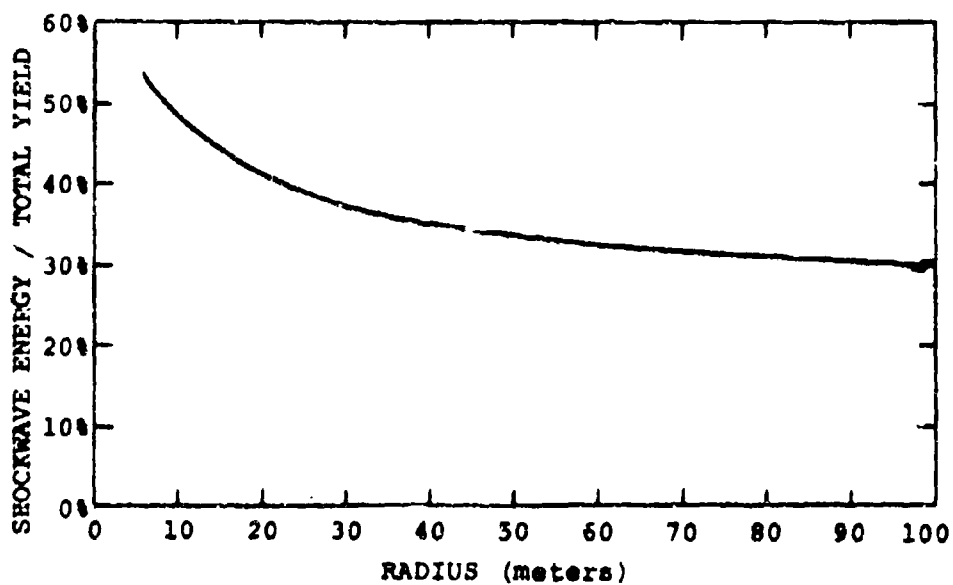
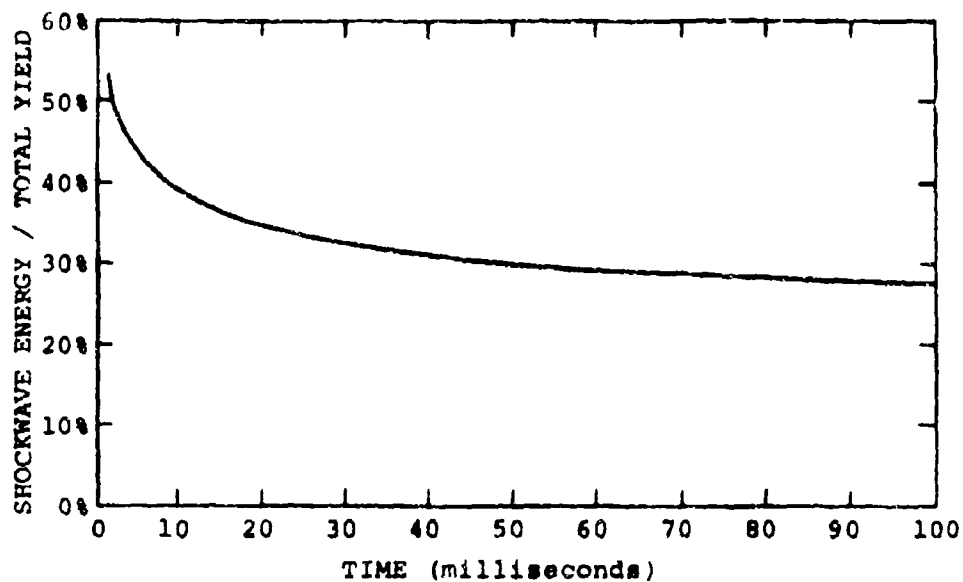


FIGURE 2: EARLY SHOCKWAVE ENERGY DISSIPATION FOR A ONE-KILOTON TNT CHARGE DETONATED UNDERWATER

The difference between the effects of a chemical underwater explosion, such as described above, and those of a nuclear or thermonuclear explosion arise from both the (usually) higher yield in the nuclear case and the far higher initial explosion energy density. The nuclear reactions may be regarded as essentially instantaneous; the materials which comprise the nuclear device (largely metals, along with the reaction products of the high-explosive stage, any unburned nuclear fuel, and the radioactive nuclear reaction products) are raised to extremely high temperatures and ionized. The earliest energy transfer mechanism to the surrounding water mass is therefore radiation; since water is opaque to bomb-temperature photons (the mean free path is only a centimeter or so), this radiation transfer process may be adequately described as "radiation diffusion". The resulting high pressure region then forms an extremely strong hydrodynamic shock wave which expands, encompassing more and more water and raising its entropy. Near the burst point, the internal energy increase per unit mass imparted to the water is sufficient that, upon expansion, the water will vaporize. This internal energy jump declines as the shock strength decreases due to its increase in surface area, however, and therefore the shock front energy density eventually becomes low enough that no further water will be vaporized. It turns out that this separation between the shock front and the bubble front occurs at a radius roughly equal to that of a spherical TNT charge of the same energy release as the nuclear explosion. Thus, at this stage, we have a physical situation not entirely unlike that of the high explosive burst at the moment when the detonation wave reaches the charge surface. The shock wave will thereafter continue to propagate outward, dissipating energy as heat at close-in distances, and rapidly becoming weaker, similar to the high-explosive case. A nuclear explosion leaves about 40% of its energy behind as "initial bubble energy"; most of the remainder is shockwave energy (of which a portion is dissipated near the burst point) and a relatively small fraction remains as energy to be released later by the decay of the radioactive

fission products. This may be compared with the 47-53% energy partition between the "bubble" and the primary shockwave for TNT (Cole, 1948); for most conventional high-explosives, the bubble energy fraction is between 40% and 60%. The difference between the high-explosive and nuclear cases is, of course, that the interior "atmosphere" of the bubble produced by a conventional underwater explosion is initially roughly homogeneous and is composed of the gaseous reaction products of the charge, whereas in the nuclear case the bubble atmosphere consists of steam and is non-homogeneous, being much hotter at the center than at the periphery.

### III. DESCRIPTION OF BUBBLE PULSATION

By the end of the dissipation phase, the shockwave has propagated well away from the "initial bubble" which consists in the conventional high explosive case of the charge's reaction products and in the nuclear case of the "potential steam" discussed above. After this point, there is a marked qualitative similarity between the two cases. If the explosion is sufficiently shallow, of course, the bubble's expansion will rupture the surface, throwing up a hollow vertical column of water, and violently expelling the bubble contents into the atmosphere. A typical example of this sort of explosion is the familiar CROSSROADS-BAKER nuclear test of 1946. For deeper explosions, however, the bubble will not vent into the air, but will continue to expand, at first rapidly, and then more and more slowly. The internal pressure and temperature will, of course, drop during this expansion, and at some point the average internal pressure will become equal to the ambient hydrostatic pressure at the burst depth. The momentum of the water rushing away from the point of burst will, however, carry the expansion even further. Eventually, the expansion will be brought to a halt by the hydrostatic pressure, and the bubble will begin to collapse. The interface will move inward with ever-increasing speed and recompression of the bubble atmosphere will occur until the motion is once again brought to a halt by the high internal pressure; thereafter, the bubble will re-expand and the whole process will be repeated. The reversal of the motion at the bubble "minimum" is so abrupt as to appear discontinuous on a time scale appropriate for the expansion-contraction cycle as a whole. On the other hand, the motion near the "maximum" is, relatively speaking, extremely smooth and leisurely; the bubble radius is more than half the value at the bubble maximum for over 90% of the period of oscillation.

During most of the expansion-contraction cycle, there is little opportunity for energy exchange between the bubble

interior and the surrounding water. Over the time periods in question, heat conduction across the bubble boundary will be entirely negligible, and hence the bubble atmosphere's expansion and recompression may be taken as adiabatic. Furthermore, a one-kiloton nuclear explosion at a burst depth of 100 meters, for example, will generate a steam bubble whose radius, at maximum expansion, is about 65 meters and whose period of oscillation is about 3.8 seconds. Thus, it can be seen that the bubble-pulsation effect is a relatively slow-motion phenomenon and is confined to a fairly small region of space, compared to the more familiar effects of the shock wave. An overall "characteristic velocity" for the oscillation may be taken as simply the maximum radius divided by the period of oscillation, or about 17 meters/second in the above typical case. This is two orders of magnitude smaller than the speed of sound in water, and consequently the water motion may be adequately treated as incompressible over most of the bubble cycle.

Near the bubble minimum, on the other hand, the assumptions of water incompressibility and adiabatic gas behavior begin to break down. First, very close to the minimum, the water velocities adjacent to the bubble interface become very high, and a weak pressure pulse is radiated away from the bubble, carrying with it a few percent of the bubble's pulsation energy. This "bubble pulse" is somewhat broader but is much lower in amplitude than the primary shockwave. Second (and much more important), at the minimum, Taylor instability occurs at the water-bubble interface. This instability is that of capillary waves on the bubble surface; thus, the size of the perturbations is quite small compared to the bubble size even at its minimum, and furthermore, the instability is a fully three-dimensional phenomenon. The resulting interface breakdown causes the formation of a spray of water droplets which penetrate the bubble, cooling its interior. If the explosion is nuclear, this cooling will cause condensation of a portion of the steam atmosphere,

thereby causing an additional energy loss. Finally, the instability of the interface initiates the development of intense turbulence adjacent to the bubble, and the energy of this turbulence is, of course, derived from bubble energy. Thus, the second cycle of oscillation is weaker than the first, and each subsequent oscillation is damped even further. Experimental measurements have shown that if the bubble does not migrate upward appreciably due to gravity, the bubble energy available for the second cycle of oscillation is about 40% of that of the first in the high-explosive case; the second cycle energy of a steam bubble, with its condensible atmosphere, is only about 8% of the first cycle energy under the same circumstances. In the high-explosive case, the bubble may experience as many as eight or ten oscillations before becoming relatively inert; in the nuclear case, however, the steam bubble will generally condense away completely at the end of the third cycle. This behavior is illustrated in Figure 3.

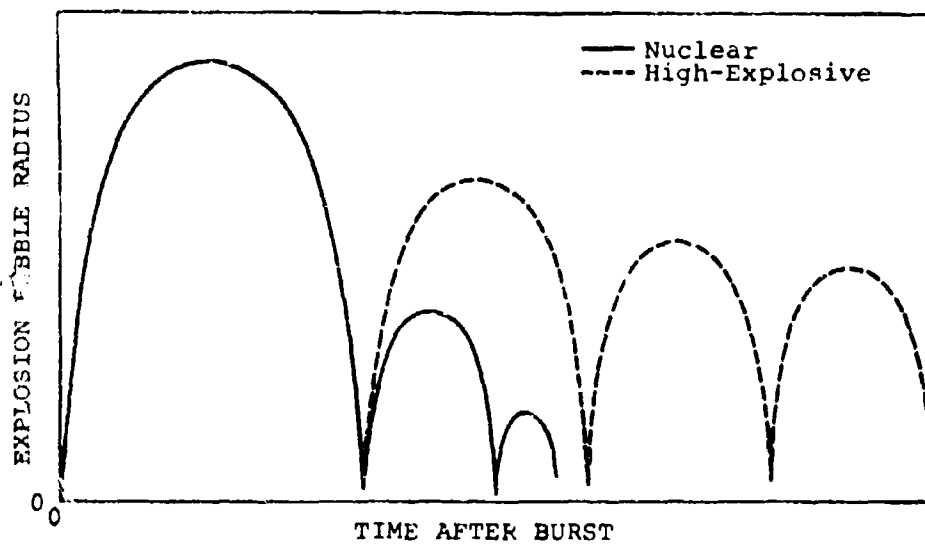


FIGURE 3: THE EFFECTS OF BUBBLE ENERGY LOSS - THE  
NON-MIGRATING CASE

#### IV. TWO-DIMENSIONAL EFFECTS

So far, it has been tacitly assumed that the bubble remains spherical in form and that its center does not move significantly during the motion. For most cases of interest, however, these assumptions are not entirely valid. As has been mentioned, if the explosion is shallow enough, the bubble may rupture the surface early in its expansion and expel its contents into the atmosphere. Furthermore, even if the explosion is well underwater, if it occurs sufficiently close to (or, particularly, in contact with) the sea bed, the motion would be expected to be influenced by this solid boundary. Therefore, in either of these cases, the motion is not one-dimensional (that is, the state of the system is not definable at a particular time in terms of the distance from the burst point alone) but is axisymmetric (requiring two space coordinates,  $r$  in the radial direction from the vertical axis of symmetry, and  $z$ , the altitude).

Even if the explosion is deep enough that the surface is not ruptured, and far enough from the sea-floor that the presence of this boundary does not significantly influence the flow, the bubble motion, in general, will still not be one-dimensional. The reason for this is the effect of gravity; that is, the buoyancy of the bubble. As a consequence of this buoyancy, the bubble will tend to float upward toward the water surface as it pulsates. The instantaneous buoyant force is given by Archimedes' principle:

$$F_b = (\rho_w - \rho_g)gV \quad (IV-1)$$

where

$\rho_w$  = density of water (constant)

$\rho_g$  = density of bubble interior

g = acceleration of gravity (constant)  
V = bubble volume.

The upward momentum generated by buoyancy up to a time  $t^*$  is therefore simply:

$$I = g \int_0^{t^*} (\rho_w - \rho_g) V dt \quad (IV-2)$$

During most of the bubble cycle, when V is large,  $\rho_g$  (the gas density) will be orders of magnitude smaller than  $\rho_w$ . Therefore, for our purposes, we may say:

$$I = \rho_w g \int_0^{t^*} V dt \quad (IV-3)$$

This momentum is accumulated with time as the motion proceeds. Near bubble maxima, when V is large, momentum is accumulated most rapidly. The "hydrodynamic mass" or "mass of moving water" is, however, also very near maxima. At the first minimum, on the other hand, the "hydrodynamic mass" is small, but possesses all the upward momentum accumulated during the first cycle, that is,

$$I = \rho_w g \int_0^T V dt = \frac{4}{3} \pi \rho_w g \int_0^T R^3 dt \quad (IV-4)$$

where T is the first oscillation period and R is the bubble radius. Therefore, the overall upward velocity is greatest at bubble minima.

The volume-time integral for the first bubble cycle in equation (IV-4) may be taken as simply proportional to the volume at the maximum times the oscillation period, for a prescribed radius-time curve:

$$\int_0^T R^3 dt = B R_{\max}^3 T \quad (IV-5)$$

where  $R_{\max}$  is the first maximum bubble radius, and the coefficient of proportionality  $B$  depends upon the exact shape of the radius-time relation for the bubble oscillation. If a "characteristic momentum" for the bubble oscillation is defined as:

$$\frac{4}{3} \pi \rho_w \frac{R_{\max}^3}{T} \quad (\text{IV-6})$$

the upward "buoyant" momentum may be normalized and presented in dimensionless form:

$$I^* = \frac{BgT^2}{R_{\max}} \quad (\text{IV-7})$$

which will be recognized as a reciprocal Froude number (increasing with increasing relative buoyancy effect). That is, two explosions which produce bubbles such that that quantity  $I^*$  is the same will experience the same relative upward migration due to gravity during the first cycle. Clearly, therefore, the quantity  $B$  (which is a measure of the shape of the radius-time curve) is an important parameter in the study of underwater explosion bubble pulsation.

It has long been recognized experimentally that if migration is strong (that is, if  $I^*$  is large), the bubble, while initially spherical, will become more and more non-spherical as the motion proceeds. After the first maximum, the bubble bottom will tend to collapse back toward the explosion point more quickly than does the top, thereby generating an upward central jet of water which collides with the bubble top just prior to the moment of maximum recompression. Therefore, at the minimum, the bubble is toroidal rather than spherical in form. If the migration strength is sufficiently great, the bubble may remain toroidal thereafter; otherwise, the central jet will dissipate upon re-expansion but may re-form at subsequent minima. For very strongly migrating bubbles, the net upward displacement by the end of the first bubble cycle may

be comparable to the first maximum bubble radius.

The MACYL6 hydrodynamic code (Pritchett, 1970a), although fairly general in application, was specifically designed to determine the bubble motion and associated phenomena following deep underwater explosions. The MACYL6 code is a computer program for solving viscous turbulent time-dependent incompressible axisymmetric fluid flows involving free surfaces. The fundamental ensemble-averaged Navier-Stokes equations which govern all such flows are numerically integrated using finite-difference methods on an Eulerian mesh of computational grid points. Free surfaces are treated using the MAC ("Marker-and-Cell") technique first developed by Welch, Harlow, Shannon and Daly (1966) at Los Alamos. In this procedure, the fluid is "tagged" with a large number of massless "marker particles" which are moved with the flow through the Eulerian mesh at each time step using velocities interpolated from nearby principal grid points. These marker particles thereby delineate the positions of the free surfaces. A heuristic model to determine the effects of turbulence was developed separately (Gawain and Pritchett, 1970) and is an integral part of the overall procedure. For application to the underwater nuclear explosion problem, the fluid is taken as initially at rest and the water surface is horizontal, but one or two "empty" cells at the explosion point contain a high internal pressure. The code then calculates the subsequent water flow in a stepwise fashion using the finite-difference forms of the governing equations and, as boundary conditions, the fact that the air pressure is constant and that the bubble internal pressure is a prescribed function of bubble volume. For all such calculations published to date, the bubble pressure - volume relation for a particular cycle of oscillation was assumed to be that of the adiabatic rarefaction and recompression of an ideal gas with  $\gamma$  (the ratio of specific heats) equal to  $4/3$ , that is,

$$pV^{4/3} = \text{constant} \quad (\text{IV-8})$$

As was discussed in section III, although the bubble's expansion and recompression may be taken as adiabatic during most of the oscillation cycle, energy is lost near the bubble minimum due to two fundamental causes. First, near the minimum, a weak pressure wave (often called the "bubble pulse" to distinguish it from the primary shockwave) is emitted from the bubble and carries away a small fraction of the bubble energy. This occurs due to the compressibility of water; near the minimum, the bubble interface velocity may instantaneously become comparable with the speed of sound in water, even though over the remainder of the pulsation velocities are far below sound speed. Second, the reversal of the motion at the minimum causes Taylor instability of the bubble-water interface, which generates intense turbulence in the water adjacent to the bubble and causes the breakdown of the interface into spray, which in turn cools the bubble interior and (for nuclear explosions) causes condensation of a fraction of the steam interior. This instability is, however, a fully three-dimensional phenomenon and the scale of size of the perturbations (i.e., the spray droplets) is far smaller than the bubble itself. It therefore seems clear that an incompressible spherically symmetric or axisymmetric treatment of the water motion cannot possibly predict the energy loss at the bubble minimum. Fortunately, there is no particular requirement for such predictions; the fractions of the bubble energy lost at each minimum have been determined experimentally and have been presented by Phillips and Snay (1968) for steam bubbles and by Snay (1952) for the conventional high-explosive case. It turns out that the fraction of the bubble energy lost at the bubble minimum declines, in general, with increasing migration strength. In the MACYL6 code, the constant in equation (IV-8) is adjusted downward at each bubble minimum in such a way that the fractions of the bubble energy lost at each minimum correspond to Snay's empirical results; thus, the decay of the bubble oscillation with time is properly reproduced in the calculations.

An earlier version of this code has been used with considerable success in the calculation of the bubble motion after the WIGWAM deep underwater nuclear explosion test of 1955 (Pritchett and Pestaner, 1969). The MACYL6 code itself has been used more recently to compute the bubble motion and subsequent flow after extremely deep underwater nuclear bursts out to several minutes after detonation (Pritchett, 1971) and is now being used to study the formation of surface waves by relatively shallow nuclear explosions. As was seen above, however, the MACYL6 code actually computes only the water flow outside the explosion bubble; the gas dynamics of the bubble interior are represented only in an approximate way (such as by equation IV-8). Although this procedure has been quite successful at accurately computing bubble motion (Pritchett, 1970b), it is certainly worthwhile to investigate the adequacy of assumptions such as (IV-8), so as to ascertain whether or not an improved "bubble interior model" can be formulated which will significantly improve the results. For this purpose, however, it is not necessary to make fully two-dimensional (that is, axisymmetric) calculations. If the one-dimensional case can be adequately treated using a particular "model" for the bubble interior, the two-dimensional case in which the bubble may become non-spherical will also be adequately described by the same sort of model.

Therefore, we will consider the case of an explosion in an unbounded mass of water in which the ambient hydrostatic pressure is everywhere the same. The effects of viscosity (which, in reality, are exceedingly small) will be neglected, and furthermore, the water outside the bubble will be considered incompressible. As was inferred in the previous discussion, this assumption is valid except for very brief time intervals near the bubble minima. In any case, the objective of this study is to determine optimum procedures for representing the effects of the bubble interior in the MACYL6 code, and MACYL6 treats the water in the incompressible approximation.

## V. SOLUTIONS NEGLECTING THE BUBBLE ATMOSPHERE

The first (and most primitive) model for the bubble interior which will be considered is that there is no bubble atmosphere at all; that is, that the motion begins with water rushing away from an infinitesimal point forming an evacuated cavity. To derive the governing equations for the resulting motion, we first impose Euler's momentum conservation equation for an incompressible fluid in spherically symmetric motion:

$$\frac{\partial u}{\partial t} + \frac{1}{r^2} \frac{\partial}{\partial r} (r^2 u^2) = - \frac{1}{\rho_w} \frac{\partial P}{\partial r} \quad (V-1)$$

where

$u$  = radial velocity

$r$  = distance from origin

$P$  = pressure

$\rho_w$  = fluid density (constant), and

$t$  = time.

Furthermore, the continuity condition is:

$$\frac{1}{r^2} \frac{\partial}{\partial r} (r^2 u) = 0 \quad (V-2)$$

If at a particular time the radius of the bubble is denoted by  $R$  and its instantaneous velocity of expansion is  $\dot{R}$ , the velocity elsewhere in the water is just:

$$u = \dot{R} (R/r)^2 \quad \text{for } r \geq R \quad (V-3)$$

as can be seen from the above continuity condition. Inserting this result into the momentum equation, we immediately obtain:

$$\ddot{R} \left(\frac{R}{r}\right)^2 + 2 \frac{\dot{R}^2 R}{r^2} - 2 \frac{\dot{R}^2 R^4}{r^4} + \frac{1}{\rho_w} \frac{\partial P}{\partial r} = 0 \quad (V-4)$$

where

$$\ddot{R} = \frac{d\dot{R}}{dt} = \frac{d^2R}{dt^2}$$

as the governing equation.

To eliminate pressure, we try a solution of the form:

$$\frac{P}{\rho_w} = a_0 + \frac{a_1}{r} + \frac{a_2}{r^2} + \frac{a_3}{r^3} + \frac{a_4}{r^4} \quad (V-5)$$

so that:

$$\frac{1}{\rho_w} \frac{\partial P}{\partial r} = -\frac{a_1}{r^2} - \frac{2a_2}{r^3} - \frac{3a_3}{r^4} - \frac{4a_4}{r^5} \quad (V-6)$$

Substituting the above into the governing equation (V-4), we obtain:

$$a_1 = \ddot{R} R^2 + 2 \dot{R}^2 R$$

$$a_2 = a_3 = 0$$

$$a_4 = -\frac{1}{2} \dot{R}^2 R^4 \quad (V-7)$$

and therefore:

$$\frac{P}{\rho_w} = a_0 + \frac{\ddot{R} R^2}{r} + 2 \dot{R}^2 \frac{R}{r} - \frac{\dot{R}^2 R^4}{2r^5} \quad (V-8)$$

Now, at  $r = \infty$ , the pressure is simply the hydrostatic pressure,  $P_H$ :

$$P = P_H \quad \text{at } r = \infty \quad (V-9)$$

and thus:

$$a_0 = \frac{P_H}{\rho_w} \quad (V-10)$$

Therefore, the pressure field is given by:

$$P = P_H + \rho_w \left( \frac{\ddot{R} R^2}{r} + 2\dot{R}^2 \frac{R}{r} - \frac{\dot{R}^2 R^4}{2r^4} \right) \quad (V-11)$$

If we define the instantaneous pressure at the hubble-water interface as  $P_B$ , we may evaluate the above equation at  $r = R$  to obtain an equation of motion for the bubble:

$$\ddot{R} = \frac{P_B - P_H}{\rho_w R} - \frac{3}{2} \frac{\dot{R}^2}{R} \quad (V-12)$$

Now, if the bubble atmosphere is ignored, the bubble pressure  $P_B$  is always zero; thus, finally, we obtain:

$$\ddot{R} = - \left[ \frac{P_H}{\rho_w R} + \frac{3}{2} \frac{\dot{R}^2}{R} \right] \quad (V-13)$$

It is also feasible to derive the governing equation from the energy principle. The total energy in the system remains constant, and is composed of two terms; the kinetic energy of the moving water, and the total work done against external forces (in this case, the hydrostatic pressure);

$$E_0 = E_K + W \quad (V-14)$$

The total kinetic energy may be evaluated by

$$E_K = \frac{1}{2} \int \rho_w u^2 dv = 2\pi\rho_w \int_R^\infty r^2 u^2 dr \quad (V-15)$$

Using the continuity condition (equation V-3 above), this becomes:

$$\begin{aligned} E_K &= 2\pi\rho_w \dot{R}^2 R^4 \int_R^\infty \frac{dr}{r^2} \\ &= 2\pi\rho_w \dot{R}^2 R^3 \end{aligned} \quad (V-16)$$

The work done against hydrostatic pressure to expand the bubble from radius  $R_0$  to radius  $R$  is simply:

$$W = \int_{R_0}^R P_H A \, dR$$

where  $A$  is the instantaneous bubble area, or:

$$\begin{aligned} W &= 4\pi P_H \int_{R_0}^R R^2 dR \\ &= \frac{4}{3} \pi P_H (R^3 - R_0^3) \end{aligned} \quad (V-17)$$

In the present case, the bubble starts from zero radius, and therefore the total work done is just:

$$W = \frac{4}{3} \pi P_H R^3 \quad (V-18)$$

Therefore, the energy equation becomes:

$$E_0 = 2\pi\rho_w \dot{R}^2 R^3 + \frac{4}{3} \pi P_H R^3 \quad (V-19)$$

If this equation is differentiated with respect to time, the result is:

$$0 = 4\pi\rho_w \ddot{R} \dot{R} R^3 + 6\pi\rho_w \dot{R}^3 R^2 + 4\pi P_H \dot{R} R^2$$

which may be solved algebraically for  $\ddot{R}$ :

$$\ddot{R} = - \left[ \frac{P_H}{\rho_w R} + \frac{3}{2} \frac{\dot{R}^2}{R} \right]$$

which is identical to the governing equation derived from the momentum principle (equation V-13).

A special case of the "gasless" bubble solution is that which is obtained if the hydrostatic pressure is ignored; that is, in terms of energy equation, the kinetic energy remains constant:

$$E_0 = 2\pi\rho_w \dot{R}^2 R^3 \quad (V-20)$$

for which the solution may be obtained analytically:

$$R = \left( \frac{25E_0}{8\pi\rho_w} \right)^{1/5} \times t^{2/5} \quad (V-21)$$

In this case, the bubble radius increases monotonically with time, and no bubble pulsation occurs due to the absence of hydrostatic pressure. This result is approximately valid at early times, but becomes worse and worse as the bubble grows and the work done against hydrostatic pressure becomes an important term in the bubble energy balance.

This case is interesting, however, in that it permits a rough estimate of the adequacy of the incompressible assumption. The error may be estimated as being of the order of the square of the Mach number based upon the interface velocity, which may be shown from (V-21) to be:

$$M^2 = \frac{1}{2\pi} \frac{E_0}{\rho_w R^3 C^2} \quad (V-22)$$

where C is the speed of sound in water. This quantity is plotted in Figure 4 for the one-kiloton case discussed earlier; as can be seen, at a radius corresponding to the TNT-equivalent charge radius, the local Mach number is significantly less than unity. Similarly, the square of the local Mach number as a function of time is:

$$M^2 = \frac{4}{25C^2} \left( \frac{25}{8\pi\rho_w} E_0 \right)^{2/5} \times t^{-6/5} \quad (V-23)$$

which is plotted for a one-kiloton explosion in Figure 5. The incompressible approximation is clearly warranted after about 5 or 10 milliseconds; the overall oscillation period of the explosion bubble is several seconds. Therefore, these results tend to support the conclusion drawn earlier that the water flow around the bubble may be adequately treated as incompressible motion.

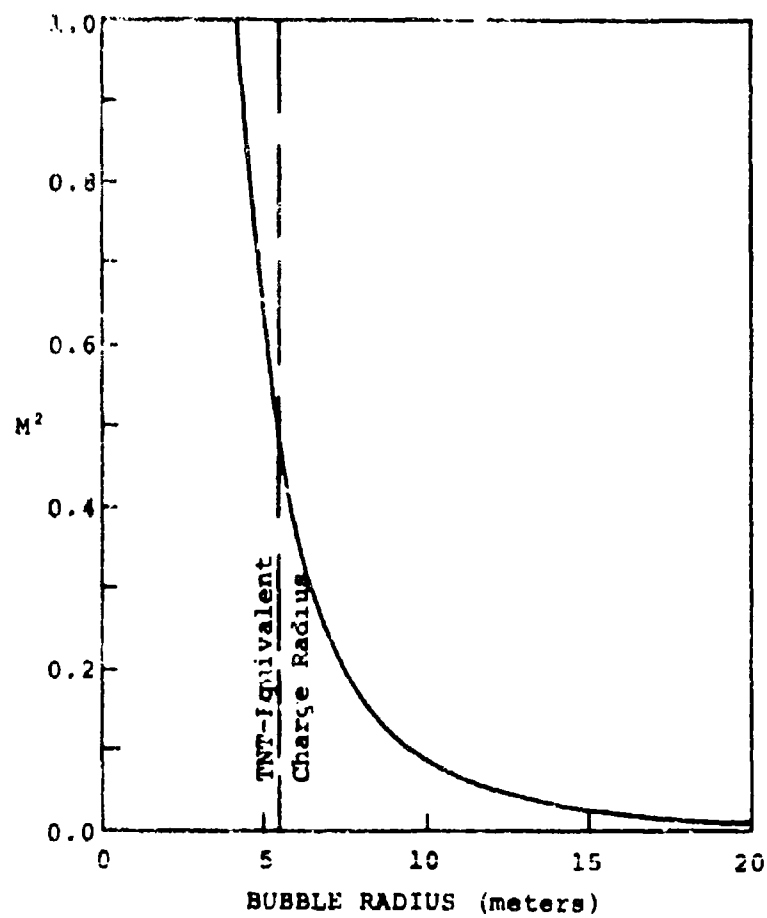


FIGURE 4: THE GASLESS MODEL - SQUARE OF THE MACH NUMBER VS. BUBBLE RADIUS FOR A ONE-KILOTON UNDERWATER EXPLOSION

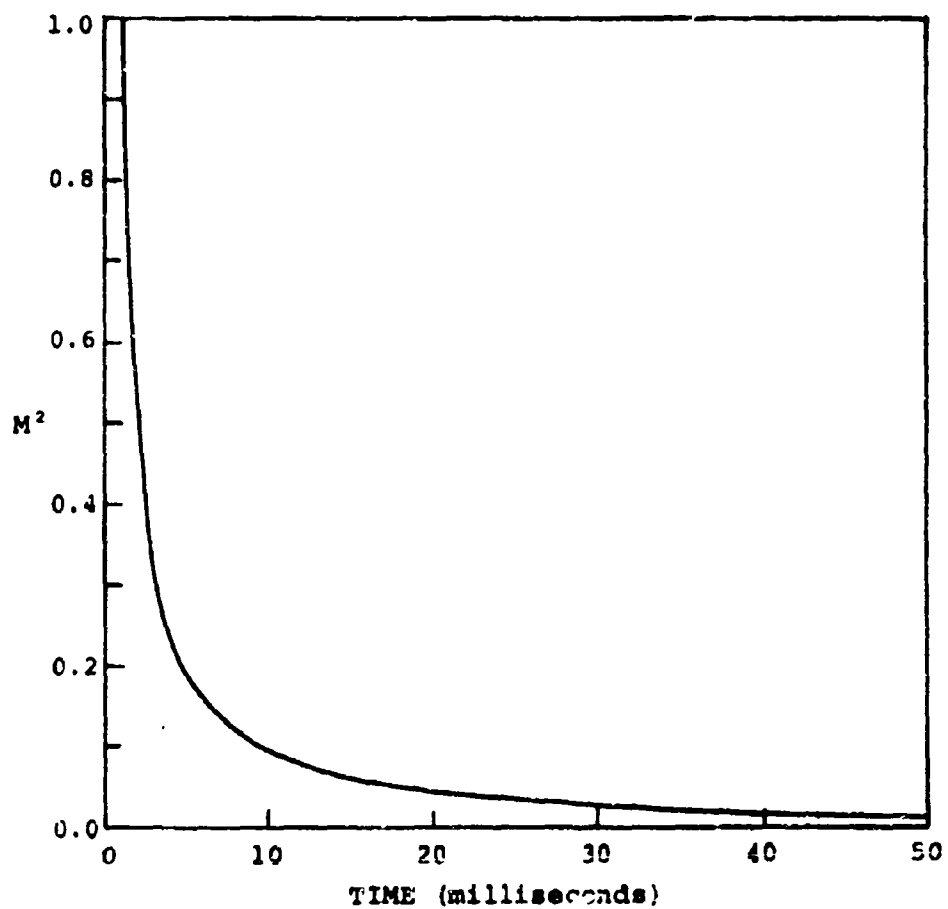


FIGURE 5: THE GASLESS MODEL - SQUARE OF THE MACH NUMBER VS. TIME FOR A ONE-KILOTON UNDERWATER EXPLOSION

If the hydrostatic pressure is non-zero, of course, the bubble will not expand indefinitely, but will oscillate in size. If a "reduced radius" and "reduced time" are defined as follows:

$$\lambda = R \left( \frac{P_H}{E_O} \right)^{1/3} \quad (V-24)$$

$$\tau = t \frac{P_H^{5/6}}{\rho_w^{1/2} E_O^{1/3}} \quad (V-25)$$

and these variables substituted into equation V-19, the energy equation may be written in dimensionless form:

$$2\pi \dot{\lambda}^2 \lambda^3 + \frac{4}{3} \pi \lambda^3 = 1 \quad (V-25)$$

where

$$\dot{\lambda} = \frac{d\lambda}{d\tau}$$

As can be seen, the maximum radius of the bubble will occur when the bubble interface velocity is zero:

$$\Lambda = \left( \frac{3}{4\pi} \right)^{1/3} = 0.620 \quad (V-26)$$

or, in dimensional form,

$$R_{\max} = 0.620 \left( \frac{E_O}{P_H} \right)^{1/3} \quad (V-27)$$

where

- $\Lambda$  = maximum dimensionless radius  $\lambda$
- $R_{\max}$  = maximum bubble radius
- $E_O$  = bubble energy (about half the total explosion energy)
- $P_H$  = hydrostatic pressure

The energy equation (V-25) may be integrated numerically: the resulting dimensionless radius-time relation is illustrated in

Figure 6. The relative contributions of the kinetic and internal energy terms to the total energy as functions of time are shown in Figure 7. As is to be expected from the form of equation V-25, the solution is symmetric around the time of the bubble maximum and there exist periodic singular discontinuities corresponding in time to the bubble minima. The period of the oscillation in dimensionless form is:

$$\delta\tau = 1.135 \quad (V-28)$$

or, in dimensional form,

$$T = 1.135 \rho_w^{1/2} E_o^{1/3} / P_H^{5/6} \quad (V-29)$$

where  $\delta\tau$  is the  $\tau$  interval between successive zeroes of  $\lambda$ , and  $T$  is the corresponding dimensional period of oscillation.

Another quantity of interest which has been discussed previously is the "characteristic velocity" associated with the bubble oscillation. This may be taken as:

$$U_c = R_{\max}/T \quad (V-30)$$

which, using V-27 and V-29, becomes:

$$U_c = \frac{\Lambda}{\delta\tau} \left( \frac{P_H}{\rho_w} \right)^{1/2} \quad (V-31)$$

so that the corresponding dimensionless parameter is:

$$\mu = \Lambda/\delta\tau = 0.547 \quad (V-32)$$

Therefore, the "characteristic velocity" is independent of the explosion yield, and depends only on the hydrostatic pressure, which in turn depends on the depth of the explosion (the water density  $\rho_w$  is assumed constant). Numerically, this characteristic

FIGURE 6: THE GASLESS MODEL - THE DIMENSIONLESS BUBBLE RADIUS - TIME RELATION

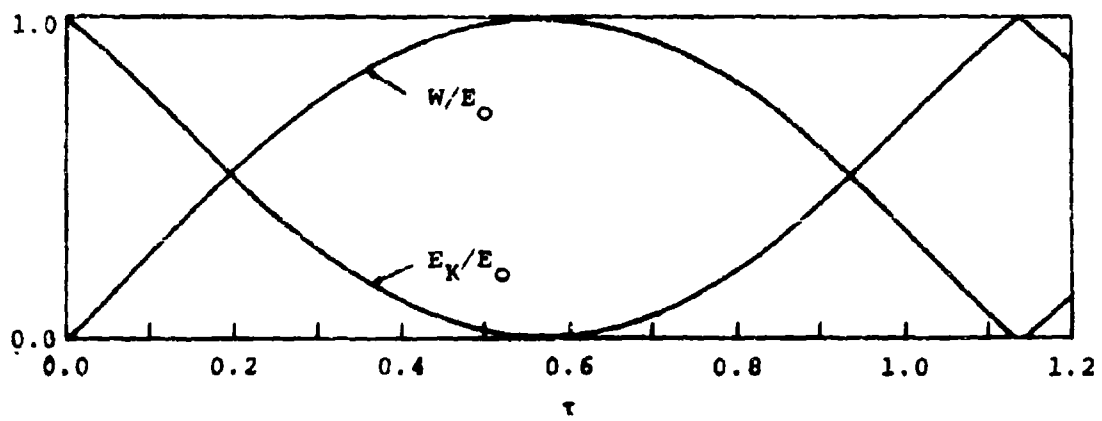
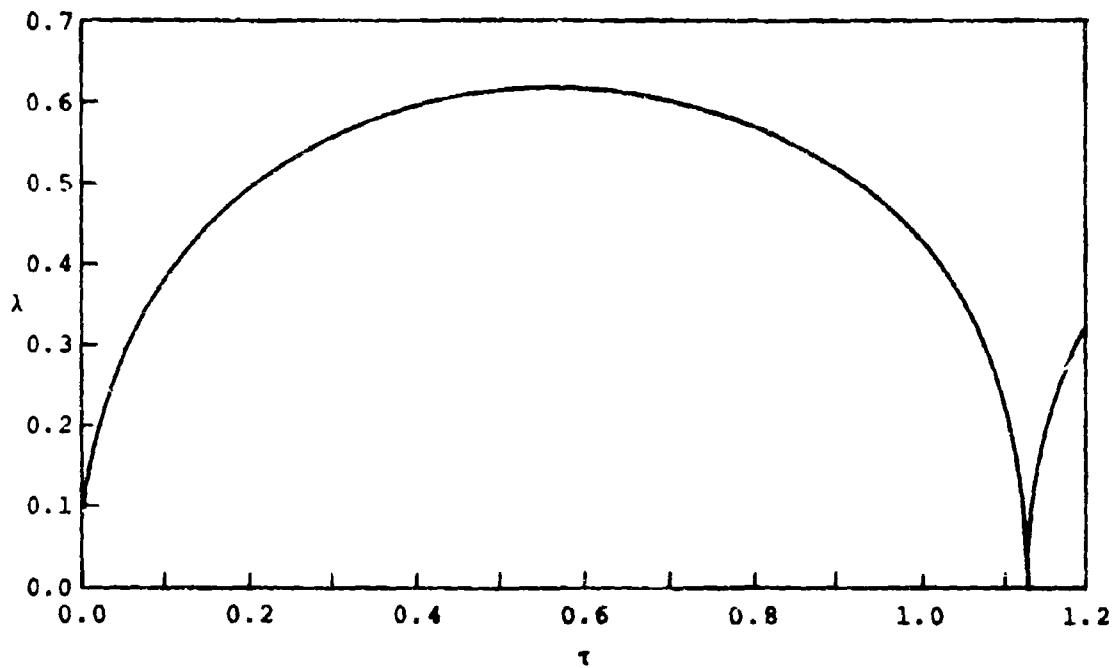


FIGURE 7: THE GASLESS MODEL - THE BUBBLE ENERGY BALANCE

velocity is fairly low, as discussed in section III, and is far below the speed of sound. Typical values for various explosion depths, assuming that  $\rho_w = 1000 \text{ kg/m}^3$ ,  $g = 9.8 \text{ m/sec}^2$ , and that the air pressure over the water is one atmosphere ( $1.013 \times 10^5 \text{ newtons/m}^2$ ) are listed in the following table:

Burst Depth (Meters)	Characteristic Velocity (Meters/Sec)	Square of Overall Mach Number
10	7.7	$2.7 \times 10^{-5}$
30	10.9	$5.3 \times 10^{-5}$
100	18.0	$1.4 \times 10^{-4}$
300	30.2	$4.1 \times 10^{-4}$
1000	54.5	$1.3 \times 10^{-3}$
3000	94.1	$3.9 \times 10^{-3}$

Thus it seems clear that water compressibility effects are not important, even for explosions at very great depths.

One other parameter required for the proper description of the bubble oscillation is the quantity B, which is needed to determine the upward momentum generated by the bubble due to buoyancy. B is defined as (see equation IV-5):

$$B \equiv \frac{\int_0^T R^3(t) dt}{R_{\max}^3 T} = \frac{\int_0^{\delta\tau} \lambda(\tau)^3 d\tau}{\lambda^3 \delta\tau}$$

The upward momentum generated by the bubble during the first cycle of oscillation in normalized form is (see equation IV-7):

$$I^* = B \frac{gT^2}{R}$$

and the value of B obtained from the integration of the energy equation is:

$$B = 0.625.$$

The very nature of the governing equation for this relatively simple case assures that the radius-time relation which results is a universal function. In the more complicated treatments considered in the next few sections, the radius-time relation will be found to depend on various parameters, so that the constants which characterize the radius-time function, that is,

$$\Lambda = 0.620 \quad (V-33)$$

$$\delta\tau = 1.135 \quad (V-34)$$

$$\mu = 0.547, \text{ and} \quad (V-35)$$

$$B = 0.625 \quad (V-36)$$

will become functions of those parameters. In general, however, the same system of nomenclature will be retained, so that results may be readily compared with the present case.

## VI. THE IDEAL GAS MODEL

In the case just discussed, the internal pressure of the bubble was approximated as zero. The bubble pressure is, in fact, low compared to hydrostatic pressure during most of the bubble cycle. None the less, it seems clear that the solution could be improved if some plausible method were used to simulate the effects of the gas inside the bubble.

In particular, if we begin with a sphere of compressed ideal gas with volume  $V_0$  and with the fluid initially at rest, the gas internal pressure may be defined by:

$$P_B V^\gamma = P_0 V_0^\gamma = \text{constant} \quad (\text{VI-1})$$

that is, an adiabatic expansion. Here,  $P_B$  is the pressure associated with bubble volume  $V$ , and  $P_0$  is the initial pressure;  $\gamma$  (the ratio of specific heats) characterizes the gas. Furthermore, it will be assumed that the gas remains homogeneously distributed within the bubble throughout the motion, and therefore:

$$u = \dot{R} \frac{r}{R} \quad \text{for } r < R \quad (\text{VI-2})$$

As before, of course, the velocity field outside the bubble is:

$$u = \dot{R} \left( \frac{R}{r} \right)^2 \quad \text{for } r \geq R \quad (\text{VI-3})$$

If the initial density of the gas is denoted by  $\rho_E$ , then the gas density inside the bubble at any time is:

$$\rho_g = \rho_E \left( \frac{R_0}{R} \right)^\gamma \quad \text{for } r < R \quad (\text{VI-4})$$

and, of course, the water density is:

$$\rho_w = \text{constant} \quad \text{for } r \geq R \quad (\text{VI-5})$$

The energy balance now consists of four components:

$$E_{KG} + E_{KW} + E_I + W = \text{constant} \quad (\text{VI-6})$$

that is, the kinetic energy of the expanding gas, the water kinetic energy, the internal (heat) energy of the bubble atmosphere and the work done against hydrostatic pressure. Two of these have already been worked out (see equations V-15 through V-17):

$$E_{KW} = 2\pi\rho_w \dot{R}^2 R^3 \quad (\text{VI-7})$$

$$W = \frac{4}{3} \pi P_H (R^3 - R_0^3) \quad (\text{VI-8})$$

The gas kinetic energy is just:

$$\begin{aligned} E_{KG} &= \frac{1}{2} \int_{\text{bubble interior}} \rho_g u^2 dv \\ &= 2\pi\rho_g \frac{\dot{R}^2}{R^2} \int_0^R r^4 dr \\ &= \frac{2}{5} \pi\rho_g \dot{R}^2 R^3 \end{aligned}$$

and, using equation (VI-4)

$$E_{KG} = \frac{2}{5} \pi\rho_g R_0^3 \dot{R}^2 \quad (\text{VI-9})$$

The internal energy of the gas is simply:

$$E_I = \frac{PV}{\gamma-1} \quad (\text{VI-10})$$

Inserting (VI-1), this may be written:

$$E_I = \frac{4\pi}{3(\gamma-1)} \frac{P_O R_O^3 \gamma}{R^3 (\gamma-1)} \quad (\text{VI-11})$$

Initially, the system is at rest and no work has yet been done against external forces. Therefore, the total energy at  $t = 0$  (the constant on the right in equation VI-6) is just the total internal energy initially present:

$$E_{I_0} = \frac{P_O V_O}{(\gamma-1)} = E_{KG} + E_{KW} + E_I + W \quad (\text{VI-12})$$

The bubble oscillation energy  $E_O$  is just the amount by which the initial internal energy exceeds the internal energy required to maintain the bubble against the ambient hydrostatic pressure:

$$\begin{aligned} E_O &= E_{I_0} - \frac{P_H V_O}{(\gamma-1)} \\ &= \frac{(P_O - P_H) V_O}{(\gamma-1)} \\ &= \frac{4\pi}{3(\gamma-1)} (P_O - P_H) R_O^3 \end{aligned} \quad (\text{VI-13})$$

Thus, for example, if the bubble oscillation energy  $E_O$  were zero, the initial bubble pressure would equal hydrostatic pressure and no motion would occur. The energy equation may now be expressed explicitly by assembling equations VI-7, -8, -9, -11, -12, and -13:

$$\begin{aligned} E_O &= 2\pi\rho_W \dot{R}^2 R^3 + \frac{2}{3} \pi\rho_E \dot{R}^2 R_O^3 + \frac{4\pi}{3(\gamma-1)} \frac{P_O R_O^3 \gamma}{R^3 (\gamma-1)} \\ &\quad + \frac{4}{3} \pi P_H (R^3 - R_O^3) - \frac{4\pi}{3(\gamma-1)} P_H R_O^3 \end{aligned} \quad (\text{VI-14})$$

which may be compared with the energy equation for the previous "gasless" case (V-19). The corresponding momentum equation is simply (compare to V-13):

$$\ddot{R} \left( 1 + \frac{1}{5} \frac{\rho_g}{\rho_w} \right) = \frac{P_B - P_H}{\rho_w R} - \frac{3}{2} \frac{\dot{R}^2}{R} \quad (\text{VI-15})$$

Making use of (VI-1) and (VI-4), this becomes

$$\ddot{R} = \frac{1}{R} \left[ \frac{1}{\rho_w} \left( P_O \left( \frac{R_O}{R} \right)^{\gamma} - P_H \right) - \frac{3}{2} \frac{\dot{R}^2}{R} \right] / \left[ 1 + \frac{1}{5} \frac{\rho_E}{\rho_w} \left( \frac{R_O}{R} \right)^3 \right] \quad (\text{VI-16})$$

The terms involving  $\rho_E$  reflect the inertial effects of the gas inside the bubble. For example, the ratio of the gas kinetic energy to that of the water is:

$$\frac{E_{KG}}{E_{KW}} = \frac{1}{5} \frac{\rho_E}{\rho_w} \left( \frac{R_O}{R} \right)^3 \quad (\text{VI-17})$$

For nuclear explosions, of course, the initial bubble density ( $\rho_E$ ) would be taken as the same as that of water ( $\rho_w$ ). Even for high explosives,  $[\rho_E/\rho_w]$  will rarely exceed 1.6 or so. Furthermore, over most of the bubble oscillation,  $R$  is vastly greater than  $R_O$ . Therefore, it would seem warranted at this stage to neglect gas inertial effects; the effect of this approximation will be examined later in this section.

If all terms involving the gas density are neglected, the energy equation becomes:

$$E_O = 2\pi \rho_w \dot{R}^2 R^3 + \frac{4}{3} \pi \left[ \frac{R_O^3}{\gamma-1} \left( P_O \left( \frac{R_O}{R} \right)^{\gamma-1} - P_H \right) + P_H (R^3 - R_O^3) \right] \quad (\text{VI-18})$$

and, for the momentum equation:

$$\ddot{R} = \frac{1}{R} \left[ \frac{1}{\rho_w} \left( P_O \left( \frac{R_O}{R} \right)^{\gamma} - P_H \right) - \frac{3}{2} \frac{\dot{R}^2}{R} \right] \quad (\text{VI-19})$$

If the governing equation is non-dimensionalized in the same way as was done in the previous section for the evacuated bubble case by the introduction of the dimensionless bubble radius ( $\lambda$ ) and the dimensionless time ( $\tau$ ), defined by:

$$R = \lambda \left( \frac{E_0}{P_H} \right)^{1/3}$$

$$t = \tau \sqrt{\rho_w} \frac{E_0^{1/3}}{P_H^{5/6}}$$

the energy equation becomes:

$$2\pi\lambda^2\lambda^3 + \frac{4}{3} \pi \left\{ \lambda^3 \left[ 1 + \left( \frac{\lambda_0}{\lambda} \right)^{3\gamma} \frac{P_0}{(\gamma-1)P_H} \right] - \frac{\gamma}{\gamma-1} \lambda_0^3 \right\} = 1 \quad (VI-20)$$

which may be compared to equation (V-25) for the "gasless" case. The bubble energy is just:

$$E_0 = \frac{(P_0 - P_H) V_0}{\gamma - 1} = \frac{4}{3} \pi \frac{(P_0 - P_H)}{\gamma - 1} R_0^3 \quad (VI-21)$$

or, in dimensionless form,

$$\lambda_0^3 = \frac{(\gamma-1)P_H}{\frac{4}{3} \pi (P_0 - P_H)} \quad (VI-22)$$

which may be used to eliminate  $\lambda_0$  from the energy equation. To facilitate presentation, we define:

$$z \equiv \frac{E_0}{\frac{4}{3} \pi P_H R_0^3} \quad (VI-23)$$

which, for the ideal gas case under discussion, is simply:

$$z = \frac{P_0 - P_H}{(\gamma-1)P_H} \quad (VI-24)$$

The physical significance of  $\zeta$  is that it is the ratio of the bubble energy to the work required to form the initial cavity of radius  $R_0$  against hydrostatic pressure  $P_H$ . Thus,  $\zeta$  may be regarded as a measure of the "relative intensity" of the explosion, or, for a given explosive type, as inversely proportional to the hydrostatic pressure, which in turn varies with the burst depth. In particular, the range of interest of  $\zeta$  can be estimated by using TNT as a standard explosive and taking note of the fact that the initial bubble energy density for TNT is about  $3 \times 10^9$  joules/m<sup>3</sup>. Thereby, the following values of  $\zeta$  may be correlated (approximately) with explosion depth as follows:

$\zeta$	Depth (meters)
100	3000
300	1000
1000	300
3000	90
10000	20

Actually, as will be seen later on, even higher values of  $\zeta$  are of some interest, since much of the experimental information concerning bubble pulsation was collected in laboratory-scale test chambers in which a vacuum was drawn over the water to further reduce hydrostatic pressure (see for example, Buntze, 1964; Snay, 1964; Pritchett, 1966). Thus, the range of variation in  $\zeta$  could extend from about 100 to as high as 100,000.

By use of (VI-22) and (VI-24), the dimensionless energy equation (VI-20) may be written as follows:

$$2\pi\lambda^2\lambda^3 + \frac{4}{3}\pi\lambda^3 + \frac{(1 + \frac{1}{(\gamma-1)\zeta})}{(\frac{4}{3}\pi\lambda^3)^{\gamma-1}\lambda^3} - \frac{\gamma}{(\gamma-1)\zeta} = 1 \quad (VI-24)$$

As can be seen, the solution is no longer a universal function

as was true in the "gasless" case discussed in section V, but is a family of functions which depend on the values of the characteristic parameters  $\gamma$  (which characterizes the gas) and  $\zeta$  (which can roughly be correlated with explosion depth).

Equation (VI-24) was numerically integrated, using a large digital computer, for values of  $\gamma$  varying between 1.1 and 1.5, and for  $\zeta$  ranging from 100 to 100,000. Qualitatively, the radius-time relations obtained were quite similar to that of the "gasless" case discussed in section V; the result for  $\gamma = 4/3$  and  $\zeta = 3000$  is illustrated in Figure 8. The relative contributions of the various terms in the energy equation as functions of time for this case are shown in Figure 9. The principal qualitative distinction between the two cases is that the bubble radius does not drop to zero at minima. Quantitatively, however, the constants which characterized the motion in the gasless case (reduced maximum radius  $\Lambda = 0.620$ ; reduced period  $\delta\tau = 1.135$ ; reduced velocity  $\mu = 0.547$ ; "shape constant"  $B = 0.625$ ) are, in the present case, functions of both  $\gamma$  and  $\zeta$ . Contour plots of these functions are to be found in Figures 10 through 13. The reduced maximum radius  $\Lambda$  is always (as might be expected) less than that in the gasless case, and decreases with decreasing  $\gamma$  and/or  $\zeta$ . The bubble period, on the other hand, may be either greater or less than in the gasless case; the characteristic velocity  $\mu (= \Lambda/\delta\tau)$  is therefore lower than the gasless value over most of the range considered, but is slightly larger for large values of  $\gamma$  and of  $\zeta$ . The range of variation of  $\Lambda$ ,  $\delta\tau$ , and  $\mu$  over the range of interest is considerable; about 17%, 9%, and 12%, respectively. On the other hand, the "shape parameter"  $B$  is fairly insensitive to variations in  $\gamma$  and/or  $\zeta$ ; the overall range is only about 3%.

In order to evaluate the error caused by neglecting the inertial effects of the gas, the same calculations were then repeated, but using the non-dimensional forms of equations (VI-14) and (VI-15) rather than (VI-18) and (VI-19), and setting  $\rho_g$  (the

FIGURE 8: THE IDEAL GAS MODEL - THE DIMENSIONLESS RADIUS-TIME  
RELATION FOR  $\gamma = 4/3$  AND RELATIVE INTENSITY  $\zeta = 3000$

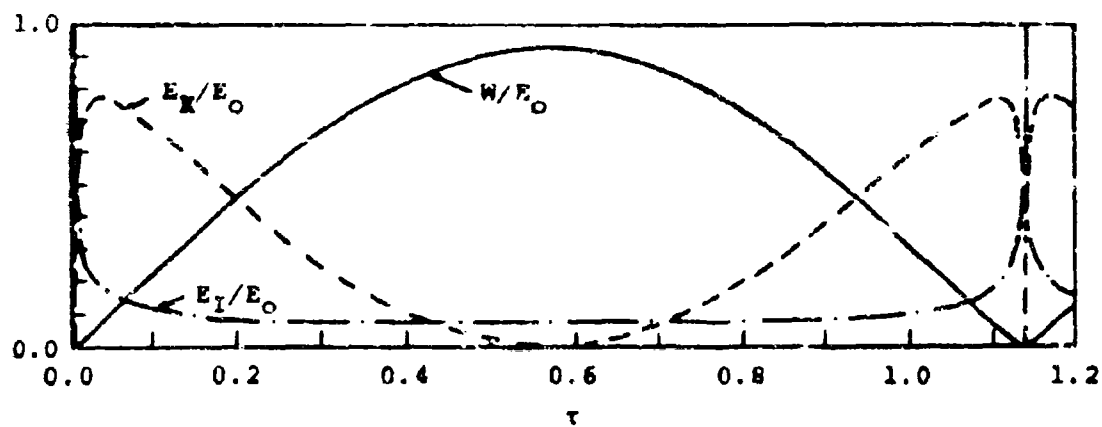
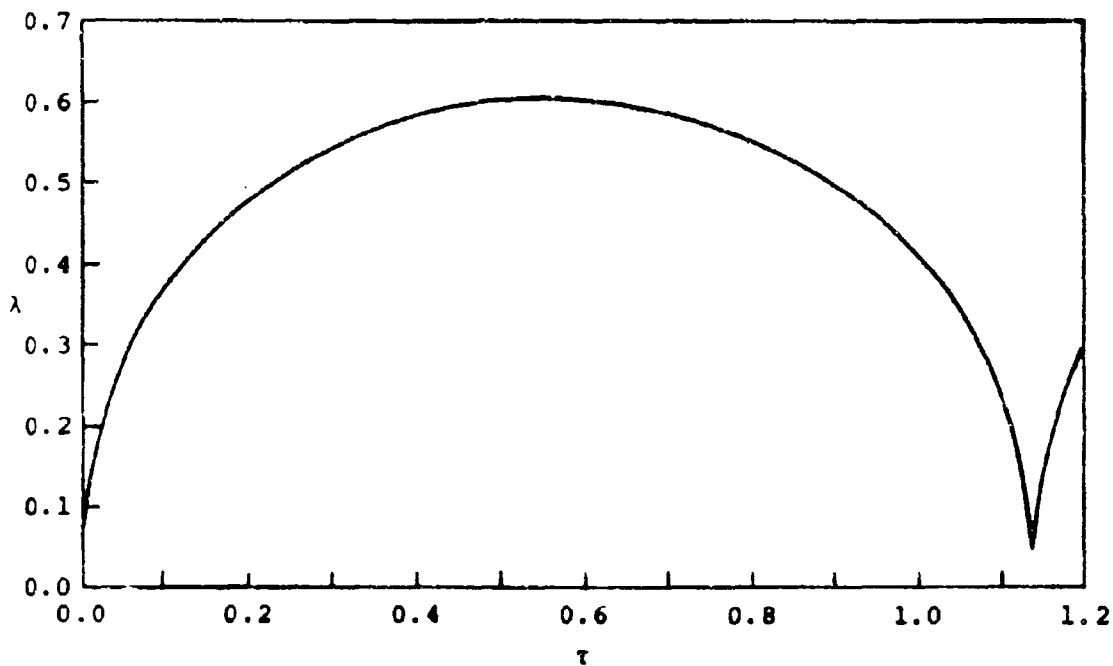


FIGURE 9: THE IDEAL GAS MODEL - THE BUBBLE ENERGY BALANCE FOR  
 $\gamma = 4/3$  AND RELATIVE INTENSITY  $\zeta = 3000$

initial gas density) equal to  $\rho_w$  (the density of water). The results were almost identical to the previous case, as shown in Figures 14 and 15. Figure 14 is a contour plot of the percentage deviation in  $\mu$  between the two cases and Figure 15 that in B. Both  $\mu$  and B were consistently lower than the results obtained using  $\rho_E = 0$ , but the deviations themselves were only fractions of a percent. An examination of the energy equation (VI-14) reveals, furthermore, that the maximum bubble radius is independent of  $\rho_E$ , since the interface velocity  $\dot{R}$  is zero at the bubble maximum. Thus, there is no difference in  $\Lambda$  between the two cases, and hence the deviation in  $\mu$  (which is just  $\Lambda/\delta\tau$ ) shown in Figure 14 is also equal, numerically, to the deviation in  $(1/\delta\tau)$ .

As these results shown, the error in  $\mu$  and B is almost independent of  $\gamma$  and depends principally on  $\zeta$ , the relative intensity of the explosion. For explosions at "reasonable" burst depths (that is,  $\zeta = 1000$  or more), the deviations are less than one-tenth of one percent; even considering the entire range down to  $\zeta = 100$ , the deviations are generally less than 1%. Therefore, the postulate made earlier that the inertial effects of the bubble atmosphere do not significantly affect the overall motion appears to be verified.

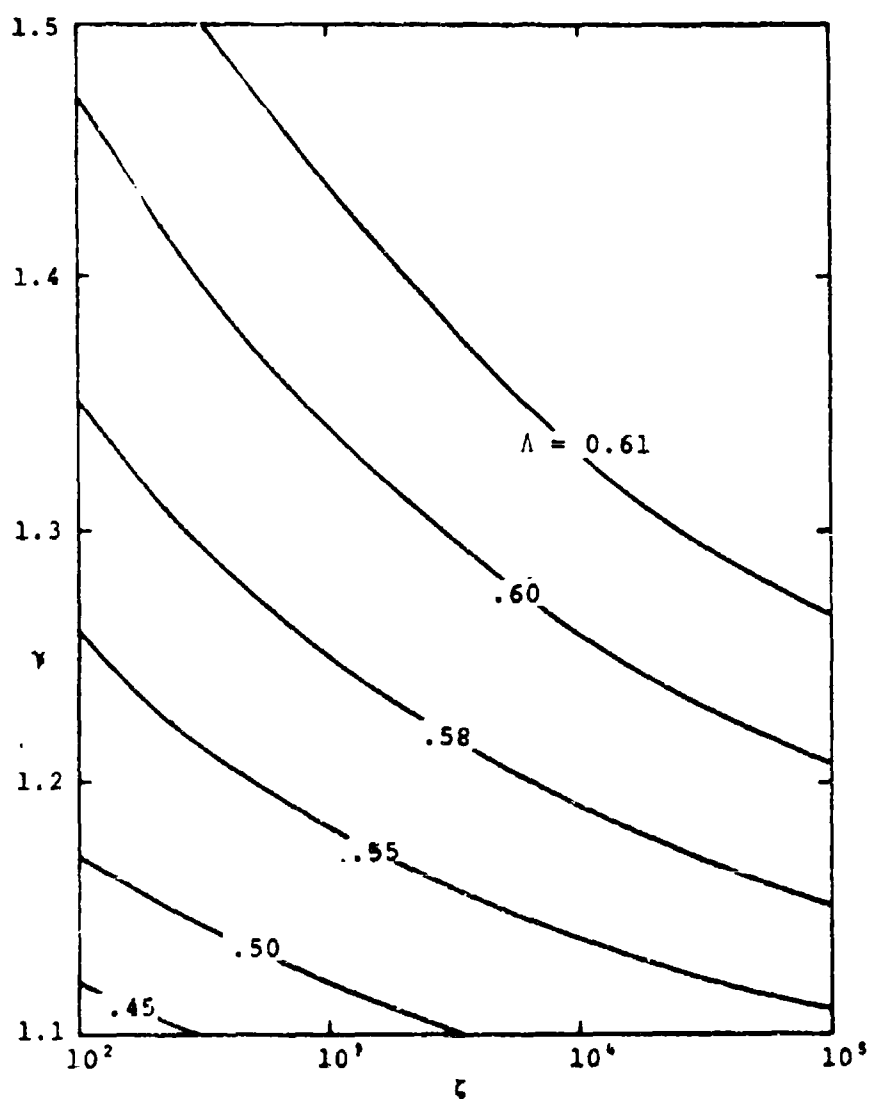


FIGURE 10: THE IDEAL GAS MODEL - THE DIMENSIONLESS MAXIMUM BUBBLE RADIUS  $\Lambda$  AS A FUNCTION OF  $\gamma$  AND  $\zeta$

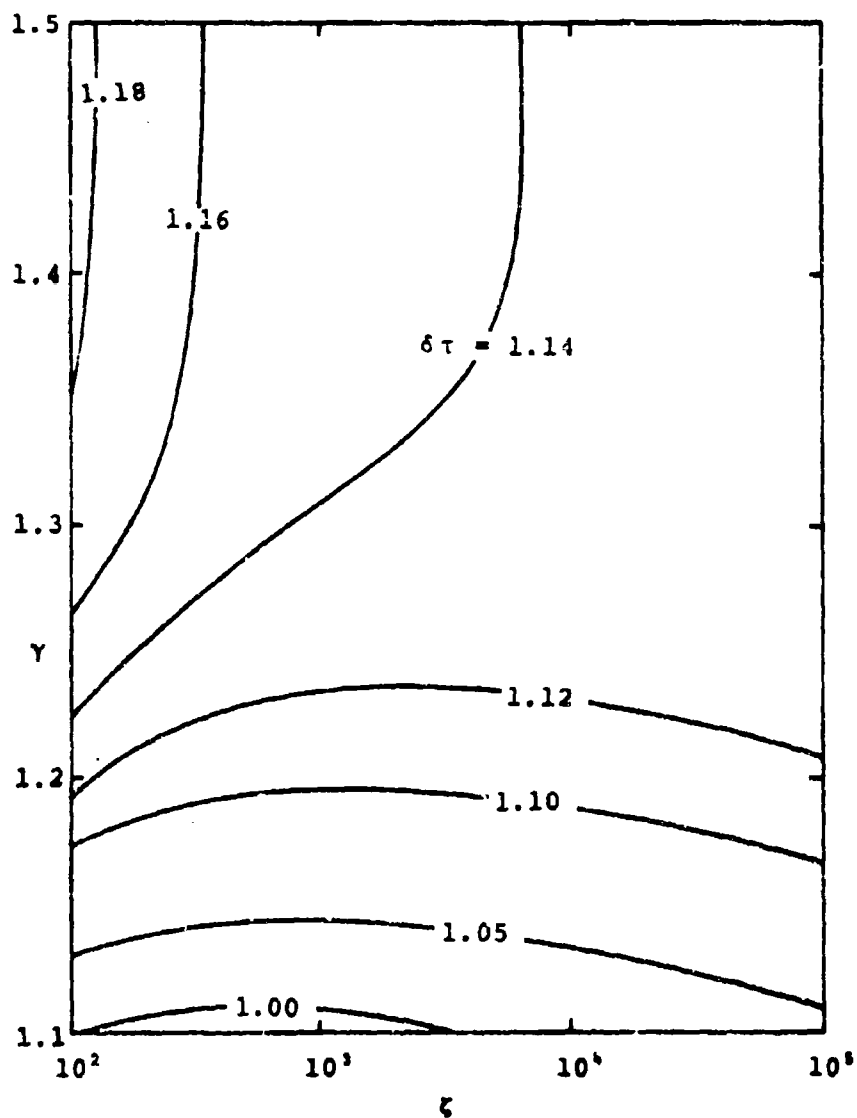


FIGURE 11: THE IDEAL GAS MODEL -- THE DIMENSIONLESS OSCILLATION PERIOD  $\delta\tau$  AS A FUNCTION OF  $\gamma$  AND  $\zeta$

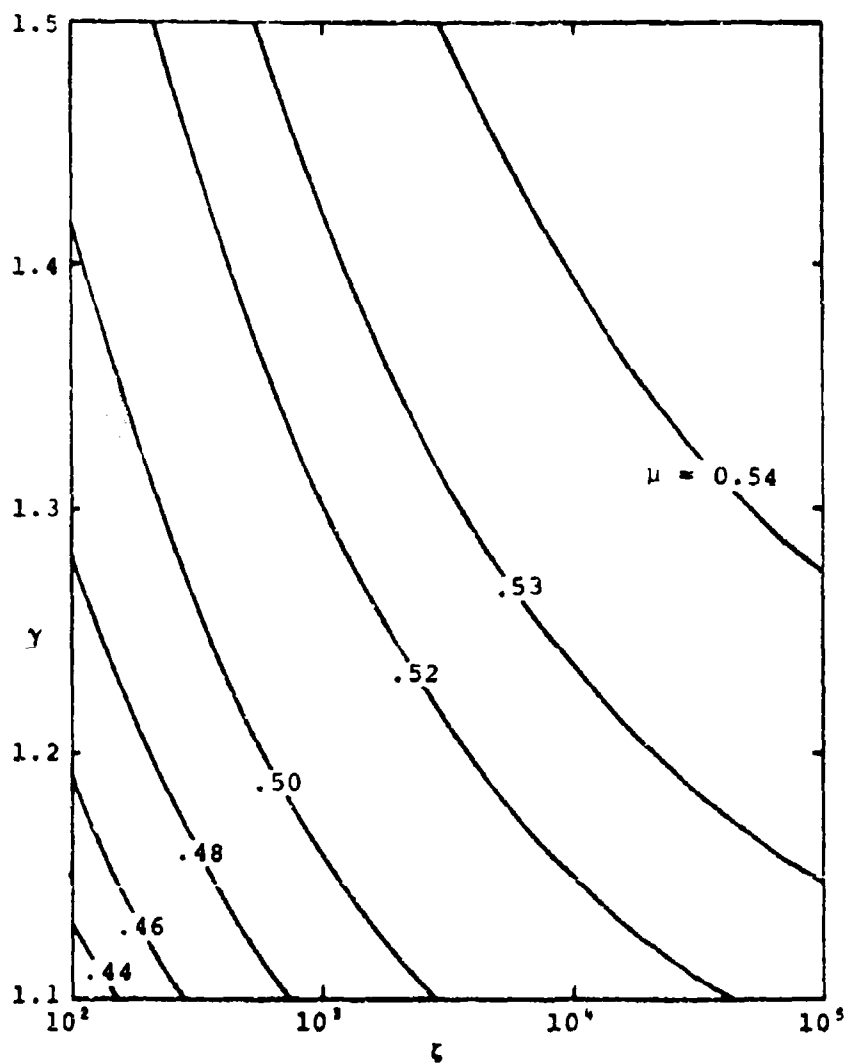


FIGURE 12: THE IDEAL GAS MODEL - THE DIMENSIONLESS CHARACTERISTIC VELOCITY  $\mu$  AS A FUNCTION OF  $\gamma$  AND  $\zeta$

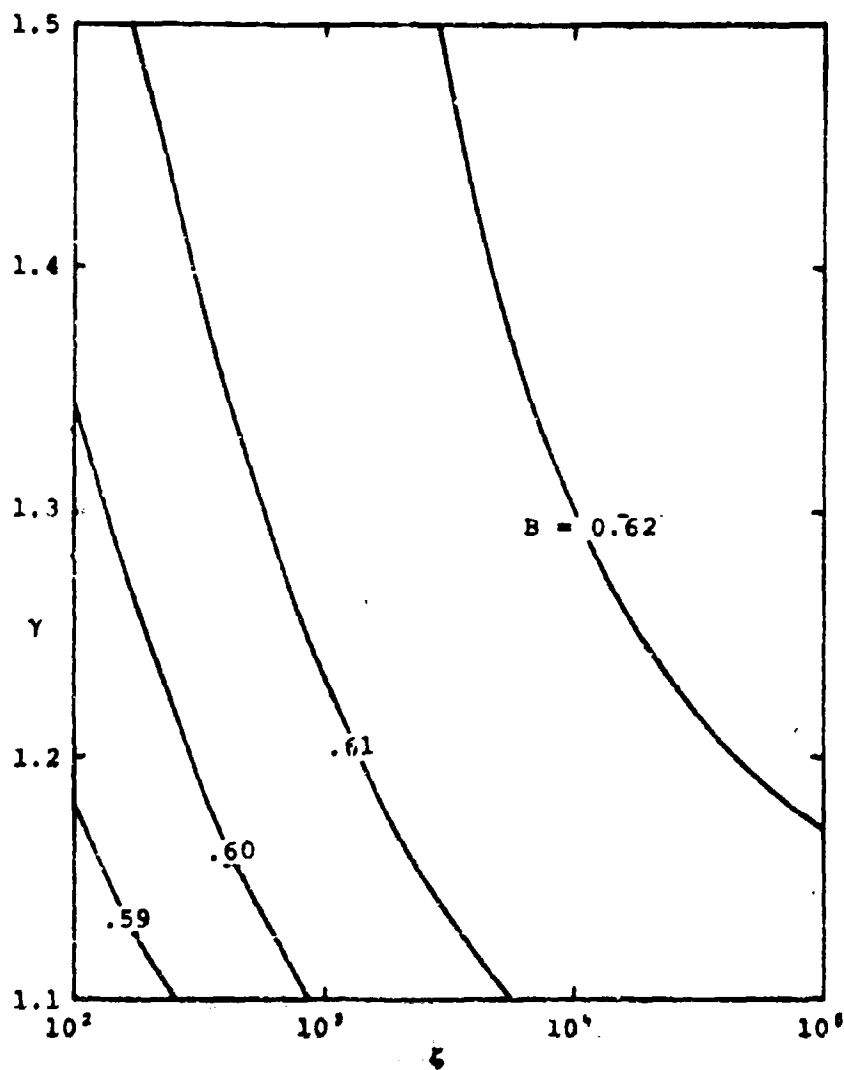


FIGURE 13: THE IDEAL GAS MODEL - THE SHAPE FACTOR  $B$  AS A FUNCTION OF  $\gamma$  AND  $\zeta$

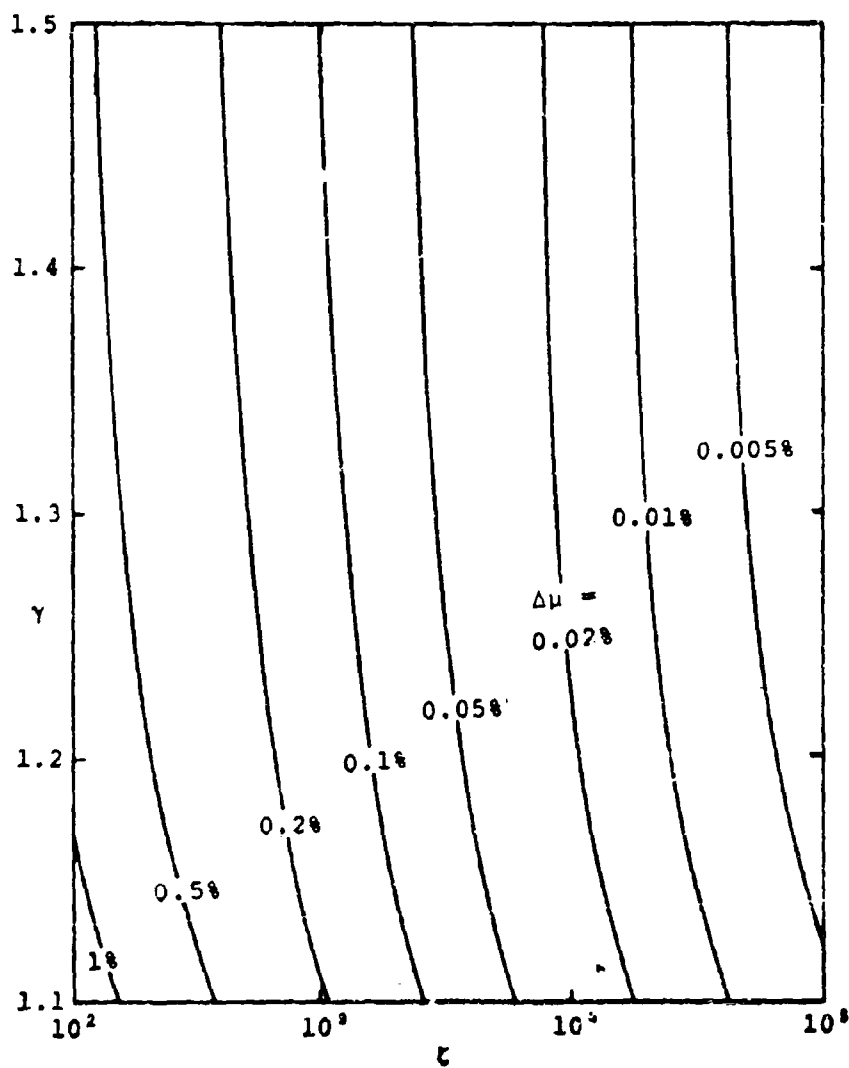


FIGURE 14: THE IDEAL GAS MODEL - THE EFFECT OF GAS INERTIA ON THE CHARACTERISTIC VELOCITY

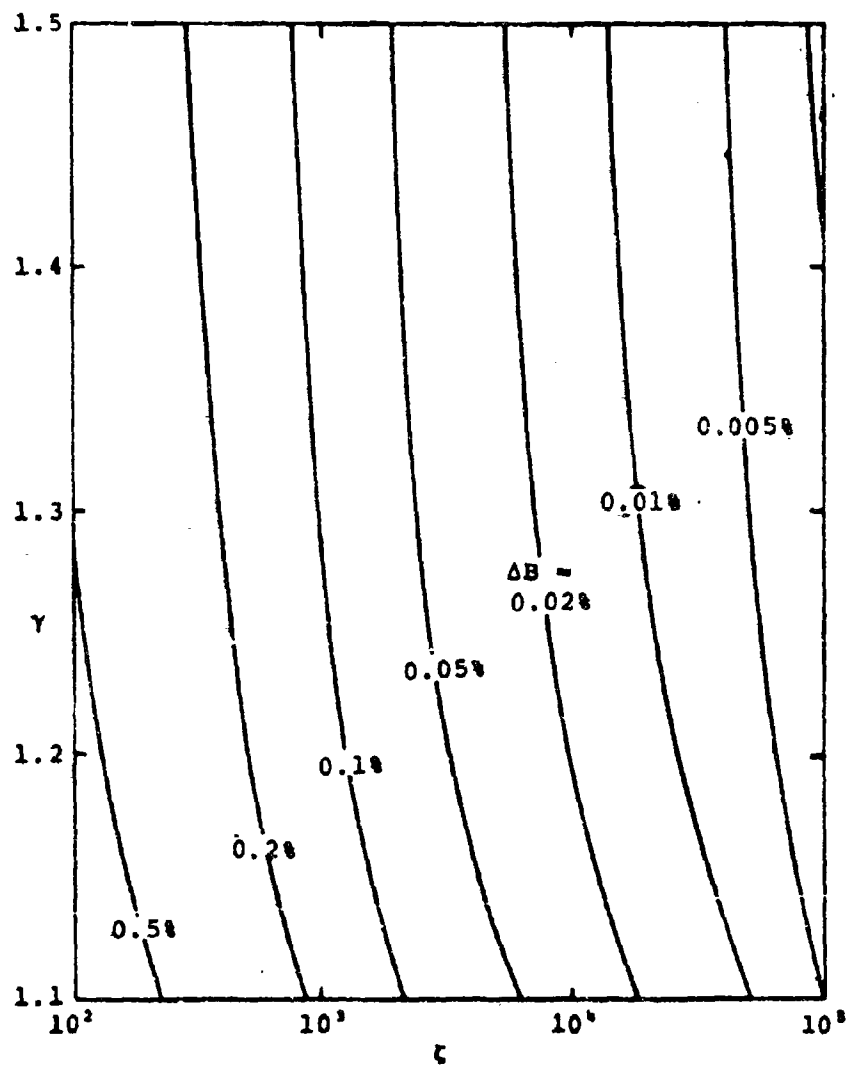


FIGURE 15: THE IDEAL GAS MODEL - THE EFFECT OF GAS INERTIA ON THE SHAPE FACTOR B

## VII. REAL-STEAM EFFECTS

In the previous section, the bubble atmosphere was treated as a homogeneous ideal gas, and the bubble pulsation effects were found to depend weakly upon  $\gamma$  (the ratio of specific heats for the ideal gas) and  $\zeta$  (the explosion intensity). It was also shown that the inertial effects of the bubble atmosphere are negligible over the range of interest of these parameters. In reality, of course, the bubble atmosphere is not an ideal gas; therefore, in this section, the effect of imposing a more realistic equation of state will be examined.

Once again, we will consider the motion of a homogeneous sphere of gas which is initially at high pressure oscillating in an incompressible fluid. The governing momentum equation for the motion is therefore the same as used previously (see equations V-12 and VI-14):

$$\ddot{R} = \frac{1}{R} \left( \frac{P_B - P_H}{\rho_w} - \frac{3}{2} \dot{R}^2 \right) \quad (\text{VII -1})$$

This equation may readily be integrated numerically if the relationship between bubble pressure ( $P_B$ ) and bubble volume is known. In section V, it was assumed that the bubble pressure was always identically zero; in section VI, the adiabatic expansion of an ideal gas was used as the model for  $P_B$ . In order to improve the treatment still further for the nuclear case, the equation of state data for  $H_2O$  collected by Bjork, Kreyenhagen, and Wagner (1969) was used.

As was done in section VI, the bubble is taken as homogeneous, the motion starts from rest, and the expansion is assumed to be adiabatic and isentropic. The initial state was taken as that corresponding to the injection of the bubble energy ( $E_0$ ) into a spherical volume of water of radius equal to that of the "equivalent TNT charge". With the equation of state specified, the only remaining variable is the hydrostatic pressure, which determines the "relative explosion intensity"

(c) discussed earlier. The equation of state data is in graphical and tabular form and is therefore rather difficult to use for calculations; consequently, only one case was actually computed, corresponding to  $\zeta = 3270$ . This value is near the middle of the range of interest, and therefore the relative deviations of the results from the cases described earlier should be typical of that to be expected from explosions at nominal burst depths. The numerical results are (in dimensionless form):

$$\Lambda = 0.6048$$

$$\delta\tau = 1.1403$$

$$\mu = 0.5304$$

$$B = 0.6198$$

The deviations of the "gasless" values obtained in section V from the above are +2.5%, -0.5%, +0.8%, and +3.1% respectively; that is, the gasless calculation tends to slightly overestimate  $\Lambda$ ,  $\mu$ , and  $B$  and to underestimate  $\delta\tau$ , the bubble period. These results for steam may also be compared with the ideal gas results obtained in section VI. The deviation of the ideal gas values from the steam values are shown in Figure 16 as functions of  $\gamma$ , the ideal-gas adiabatic exponent. As can be seen, the deviations in all four quantities are under 1% for  $\gamma$  between about 1.29 and 1.38; the best overall value would appear to be about 4/3. That is, for this case at least, the errors involved in replacing the real steam equation of state with an ideal gas with  $\gamma = 4/3$  are:

$$\Delta\Lambda = 0.19\%$$

$$\Delta\delta\tau = -0.14\%$$

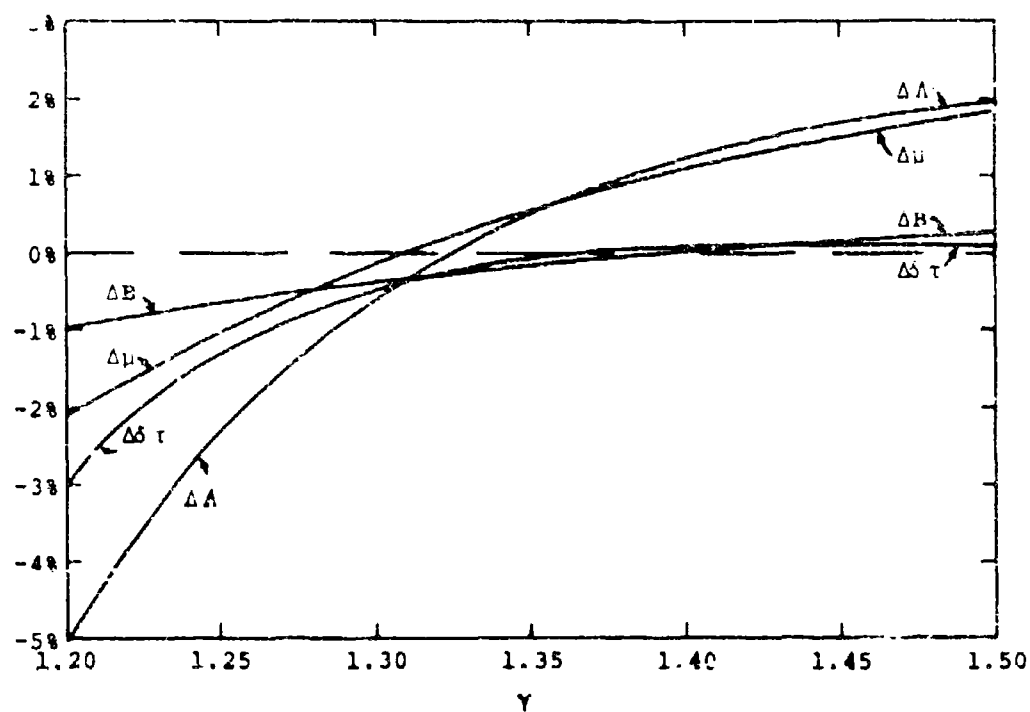


FIGURE 16: DEVIATION OF THE IDEAL GAS MODEL RESULTS FROM THE REAL-STEAM CALCULATION

$$\Delta\mu = 0.348$$

$$\Delta B = -0.248$$

The conclusion that must be drawn is that the ideal gas treatment using  $\gamma = 4/3$  is an adequate approximation to the real-steam equation of state as far as the bubble dynamics is concerned. As will be seen later on, errors of this magnitude are entirely unimportant in comparison with other effects and are, in fact, of about the same order as those introduced by neglecting the inertial effects of the bubble atmosphere which, as has been shown, are insignificant.

## VIII. BUBBLE ATMOSPHERE DYNAMICS

So far, the bubble interior has been treated as if it were homogeneous so that the internal pressure is independent of position within the bubble. As was discussed previously, this necessarily implies that the internal velocity distribution is given by:

$$u = \dot{R} \left( \frac{r}{R} \right) \quad \text{for } r < R \quad (\text{VIII-1})$$

at any time. In fact, however, it may easily be shown that the bubble will not remain homogeneous, but that conditions within the bubble will vary with position as well as with time. In the high-explosive case, the bubble may be roughly homogeneous initially, but there is certainly no guarantee that it will remain so; in the nuclear case, the bubble is markedly inhomogeneous initially. Accordingly, in this section the effects of bubble non-homogeneity will be examined in an approximate way to determine the consequences as concerns the overall water motion. As before, the water outside the bubble is treated as incompressible, but the actual detailed motion within the bubble will be taken into account in determining its radius-time history.

The motion of the gas within the bubble comprises a fully non-linear time-dependent problem in compressible dynamics and is therefore governed by Euler's equations:

$$\frac{\partial p}{\partial t} + \frac{1}{r^2} \frac{\partial}{\partial r} (r^2 \rho u) = 0 \quad (\text{VIII-2})$$

$$\frac{\partial (\rho u)}{\partial t} + \frac{1}{r^2} \frac{\partial}{\partial r} (r^2 \rho u^2) + \frac{\partial p}{\partial r} = 0 \quad (\text{VIII-3})$$

$$\frac{\partial (\rho E)}{\partial t} + \frac{1}{r^2} \frac{\partial}{\partial r} (r^2 \rho u E) + \frac{1}{r^2} \frac{\partial}{\partial r} (r^2 u p) = 0 \quad (\text{VIII-4})$$

$$P = f(\rho, H)$$

(VIII-5)

where

$u$  = velocity

$\rho$  = density

$P$  = pressure

$E$  = total energy per unit mass =  $\frac{u^2}{2} + H$

$H$  = internal energy per unit mass

$r$  = radius

$t$  = time

Equations VIII-2 through VIII-4 represent, respectively, the principles of mass, momentum, and energy conservation; equation VIII-5 is the equation of state for the gas. To solve these equations, it is convenient to transform them to a Lagrangian formulation (that is, coordinates which move with the flow, rather than remaining fixed in space). Also, as was seen in the preceding section, an ideal-gas treatment of the bubble interior is adequate, and therefore the equation of state (VIII-5) is simply:

$$P = (\gamma - 1)\rho H$$

where  $\gamma$  will be taken as 4/3.

The resulting system of equations must be solved subject to prescribed initial distributions of  $\rho$ ,  $u$ , and  $H$ , and to a boundary condition at the bubble perimeter which matches the incompressible external motion solved earlier and which may be derived from the momentum equation (VI-15), which defines the acceleration at the wall in terms of the local internal pressure, velocity, and gas density.

To solve the resulting system of equations a finite-difference method was employed which is essentially the same as

that described by Mader and Gage (1967). The hydrodynamic code is an explicit forward-time Lagrangian finite-difference scheme employing the Von Neumann-Richtmyer artificial viscosity technique to avoid instabilities associated with compression waves. The details of the method have been extensively described by Mader and will therefore not be repeated here. Two cases were actually calculated using this method; computer time limitations precluded a more extensive investigation.

For the first problem run, the bubble interior was assumed to be initially homogeneous:  $\rho$  was taken as the same as that of water, and the "explosion intensity"  $\zeta$  was 3000. The gaseous region within the bubble was divided into 100 Lagrangian computational cells; as discussed above, the effects of the water outside are taken into account by proper specification of the boundary conditions at the bubble edge. The beginning of the bubble expansion caused a rarefaction to form at the bubble edge and to propagate toward the interior; the resulting pressure wave continued to oscillate between the bubble center and bubble edge throughout the rest of the motion. Several of these interior pressure wave reverberations occurred during the first expansion, superimposed on the general overall pressure decline. The integration was carried out through 15,000 computational steps, which required about 8 minutes of CDC-6600 computer time. Calculations were carried out well beyond the point of maximum expansion and into the beginning of the bubble collapse. Although the governing equations no longer imply symmetry of the radius-time curve, the computed results themselves are symmetric to within small fractions of a percent. Accordingly, the bubble period was taken as just twice the time to maximum expansion.

The maximum bubble radius in dimensionless form computed in this way was slightly less than that obtained assuming a homogeneous bubble atmosphere, since the kinetic energy of the bubble atmosphere did not fall to zero at the maximum; the oscillating pressure disturbance mentioned above

was still present, although very weak. The dimensionless results which described the bubble radius-time relation are shown in the following table, which also lists the corresponding values for the "gasless" case and the  $\gamma = 4/3$  homogeneous ideal-gas model at the same value of  $\epsilon$ , both with and without gas inertial effects considered:

RESULT	MODEL			
	Dynamic Bubble Interior	Ideal Gas With Inertial Effects	Ideal Gas Without Inertial Effects	Gasless Model
$\Lambda$	0.6053	0.6056	0.6056	0.620
$\delta\tau$	1.1392	1.1394	1.1389	1.135
$\mu$	0.5314	0.5315	0.5317	0.547
$B$	0.6177	0.6178	0.6180	0.625

As can be seen, the consideration of the interior gas dynamics made virtually no difference to the results, and consequently the homogeneous approximation appears to be quite adequate to describe the motion. Although, in the dynamic calculation, fairly large pressure fluctuations around the mean value occurred at the bubble boundary, a sufficient number of fluctuations occurred that the average overall effect was about the same as if there had been no such fluctuations.

In the case just discussed, however, the bubble was assumed to be initially homogeneous. As was discussed earlier, a nuclear explosion would be expected to produce an "initial bubble" that is non-homogeneous, that is, hotter and less dense at the center than at the edge. To evaluate the effect of initial non-homogeneity of the bubble, the same Lagrangian hydrodynamic code was used as in the previous case, and all input conditions were the same, except that for the innermost fourth of the initial bubble radius, the density was set at one-tenth of the previous value and the internal energy per

unit mass (which is proportional to temperature) was multiplied by ten. For the outer three-fourths, the initial conditions were the same as in the previous case.

The second problem was not carried out in time as far as the first bubble maximum, since the results even at early times were essentially identical (as far as the bubble radius-time relation was concerned) with those in the previous case. The deviation never exceeded 0.04% in magnitude, and declined slowly toward zero as the computation went on. The computation was stopped at  $\tau = 0.17$ , at which time the bubble radius was 75% of the maximum value; at that point, the deviation in bubble radius between the two cases had dropped to 0.027%. The overall conclusion which must necessarily be reached from both of these calculations is that the explicit treatment of the bubble atmosphere dynamics does not significantly alter the results for the bubble radius-time relation from those obtained using the homogeneous model discussed in section VI, and that this is true regardless of the initial energy distribution within the bubble.

## IX. COMPARISONS WITH OTHER RESULTS

To evaluate the adequacy of the models discussed in the preceding sections, it is necessary to consider experimental results. As was just shown, the effects upon the radius-time relation of a non-homogeneous dynamic bubble interior are extremely slight. Furthermore, over the range of interest, the effects of the deviations of real steam behavior from  $\gamma = 4/3$  ideal gas behavior are unimportant, and the inertial effects of the bubble atmosphere are likewise negligible. Of the various models considered, only the results of the most primitive (that is, the "gasless" model of section V) differ to any significant extent from the rest, and even that case is generally within a few percent of the others. The general conclusion that must be drawn is that the bubble motion is quite insensitive to the behavior of the interior; that is, that the motion is dominated by the water flow outside the bubble rather than that of the gas inside.

In all cases considered, the water outside the bubble was assumed to be incompressible. This assumption is appropriate in view of the overall purpose of this investigation and has further been shown by various plausibility arguments to be at least approximately correct except for short time periods very near the bubble minimum. None the less, it is certainly worthwhile to determine the extent to which the ideal gas - incompressible water model represents observed explosion bubble behavior.

An enormous amount of experimental data has been acquired over the years concerning underwater explosions. Even so, precise measurements of the bubble motion are extremely difficult to obtain. For large explosions in the field, the only bubble parameter which may be readily determined is the period of oscillation, that is, the time interval between the emission of the primary shockwave and the "bubble pulse"

Proceeding page blank

pressure wave emitted at the first recompression. For high explosives fired deep enough that the presence of the free surface does not significantly affect the motion, the data may be correlated by an empirical expression of the form (Cole, 1948):

$$T(\text{sec}) = K \left( \frac{WT(\text{lb.})}{Z(\text{ft.})} \right)^{1/3} \quad (\text{IX-1})$$

where WT is the charge weight in pounds, Z is the total hydrostatic pressure measured in feet of water (that is, the depth of burst plus 34 feet representing air pressure), and K depends upon the particular type of explosive used. For TNT, for example,

$$T(\text{sec}) = 4.36 \left( \frac{WT(\text{lb.})}{Z(\text{ft.})} \right)^{1/3} \quad (\text{IX-2})$$

will predict observed bubble periods within a few percent over a wide range of charge weights and burst depths. If the initial bubble energy for TNT is taken as 47% of the total explosion energy (that is, the total minus the observed 53% shockwave fraction), the total explosion energy per unit explosive mass is assumed to be  $4.2 \times 10^6$  joules/kilograms (see section II), and water density is taken as  $1000 \text{ kg/m}^3$ , equation (IX-2) may be expressed in dimensionless form:

$$T = 1.126 \sqrt{\rho_w} E_O^{1/3} / P_H^{5/6} \quad (\text{IX-3})$$

that is,

$$\delta\tau = 1.126$$

which, as was shown in section VI (see Figure 11), agrees quite well with the values obtained from the homogeneous ideal-gas model. Over the region of interest, the ideal gas results for  $\gamma = 1.25$  (the value suggested by Snay (1957) as being most appropriate for TNT) are illustrated in Figure 17. The deviation

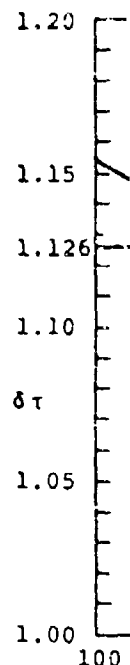


FIGURE 17

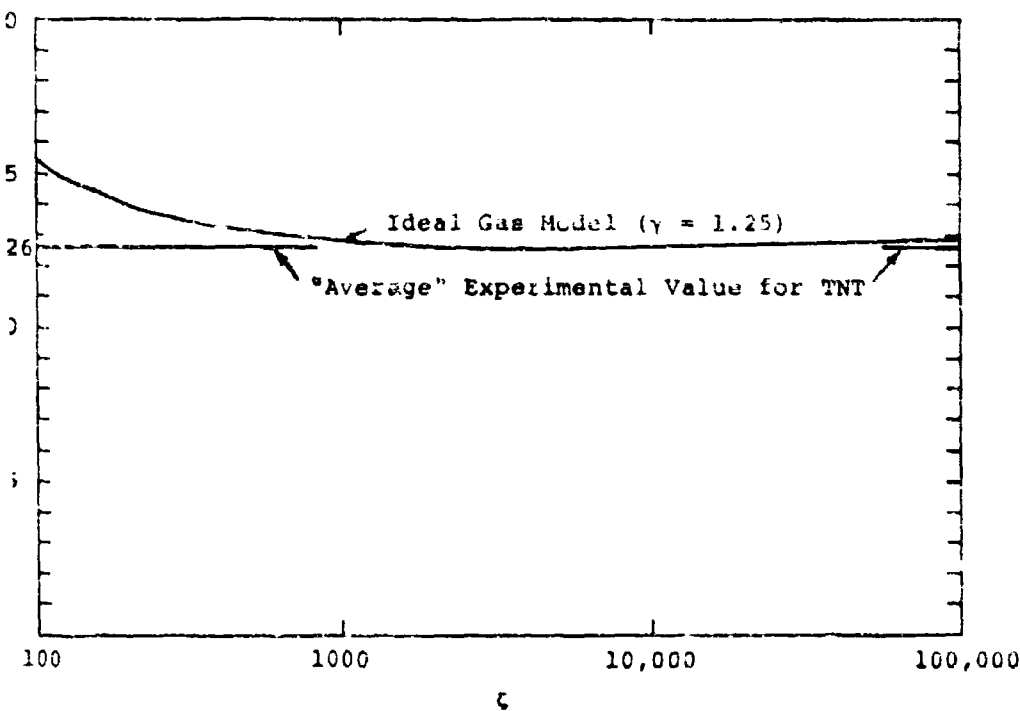


FIGURE 17: COMPARISON OF THE "AVERAGE" EXPERIMENTAL DIMENSIONLESS OSCILLATION PERIOD FOR TNT WITH IDEAL GAS MODEL RESULTS

over the range  $\zeta = 1000$  to  $\zeta = 30,000$  (the region in which most of the experimental data was acquired) is always less than 0.15%, far less than the scatter in the experimental data itself. This rather remarkable agreement between the ideal-gas results and experimental measurements for TNT is probably somewhat fortuitous, but certainly indicates that the model can adequately represent experimental results for the bubble oscillation period.

For nuclear explosions, experimental data is extremely sparse. The only available direct measurement concerning nuclear explosion bubble motion is the bubble period measured hydro-acoustically at the 1955 WIGWAM test. Operation WIGWAM consisted of the detonation of a 30 kiloton nuclear device (total energy release  $1.2 \times 10^{14}$  joules) at a depth of 610 meters in very deep water in the open sea. The first bubble period was 2.88 seconds; if the fluid density is taken as  $1025 \text{ kg/m}^3$  (an "average" value for seawater) and the initial bubble energy is taken as 40% of the total yield as discussed in section II, the dimensionless bubble period is:

$$\delta\tau = 1.137$$

which may be compared with the results of the  $\gamma = 4/3$  ideal-gas model (see Figure 18). The "reduced explosion intensity"  $\zeta$  for WIGWAM was taken as 500, based upon the assumption of an initial bubble energy density equal to that of TNT. The deviation between the two is about 1%, which is within the precision of the WIGWAM oscillation period measurement.

There are, of course, no measurements of maximum bubble radii for underwater nuclear explosions. Even for high explosives, far less data exists for the bubble radius than for the bubble period. What data is available may, however, be correlated by the empirical formula:

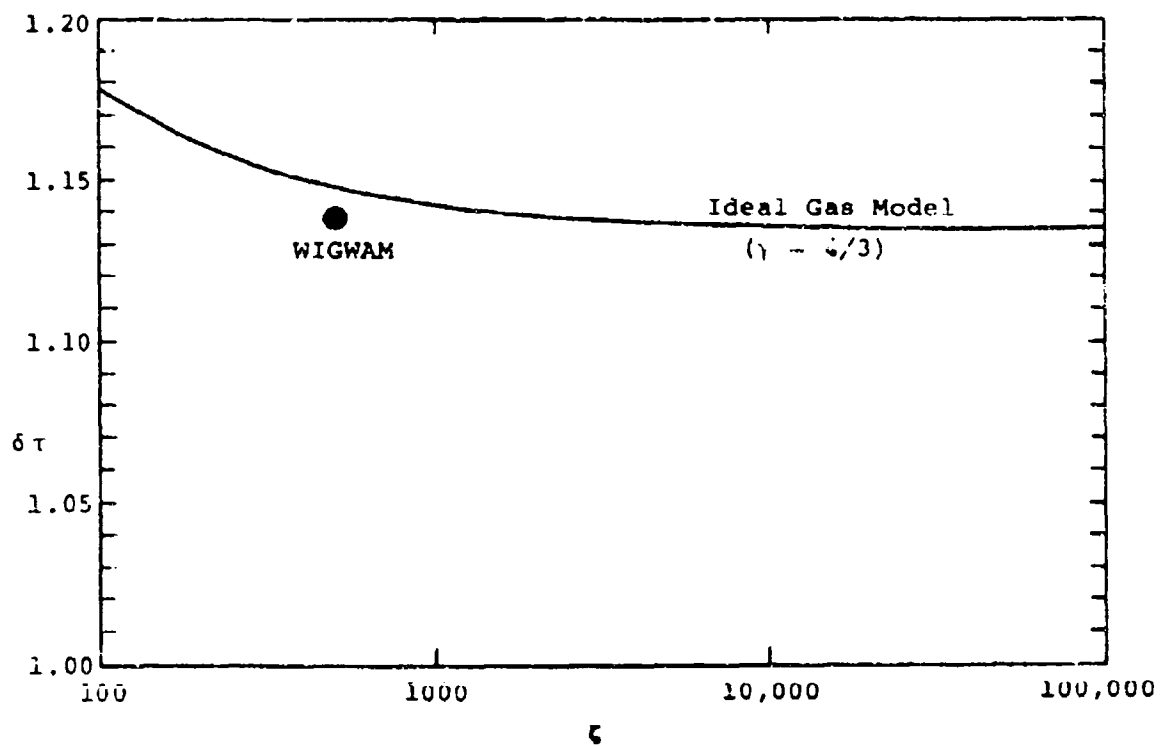


FIGURE 18: COMPARISON OF THE DIMENSIONLESS WIGWAM BUBBLE PERIOD WITH IDEAL GAS MODEL RESULTS

$$R_{\max} \text{ (feet)} = J \left( \frac{WT \text{ (lb.)}}{Z \text{ (ft.)}} \right)^{1/3} \quad (\text{IX-4})$$

which is analogous to the empirical equation for the bubble period (IX-1). For TNT,  $J = 12.6$  fits most of the available data within a few percent. This observed result may be transformed to non-dimensional form in the same way as was done with the TNT bubble period; the result is:

$$\Lambda = 0.58$$

which may be compared with the ideal-gas model results using  $\gamma = 1.25$  (see Figure 19). Again, the agreement is fairly good.

Many of the available measurements of bubble motion were taken on a laboratory scale, using very tiny charges in special test chambers in which the air pressure may be reduced to provide Froude scaling, that is, similitude of bubble buoyancy effects (see, for example, Snay, 1964; Pritchett, 1966). The purpose of these tests was, in general, to simulate the buoyant bubble migration characteristics of large explosions. For the present purpose, however, much of this data must be regarded with some suspicion. The reason is that, at low ambient hydrostatic pressures, the local pressure in the water near the bubble interface may drop below vapor pressure near bubble maxima and the surface of the bubble will then boil.

Figure 20 shows the pressure distribution in the water for an explosion at  $z = 3000$  and  $\gamma = 4/3$ . The ideal-gas model of section VI was used for this calculation, and the inertial effects of the gas were neglected. The pressure distribution was then obtained using equation V-12. As can be seen, at early times, the pressure declines with increasing distance, but once the internal pressure drops below  $P_H$  (the hydrostatic pressure), the point of lowest instantaneous pressure is directly adjacent to the bubble interface. Thus, if the interior pressure at the maximum predicted by this theory is less than the water vapor

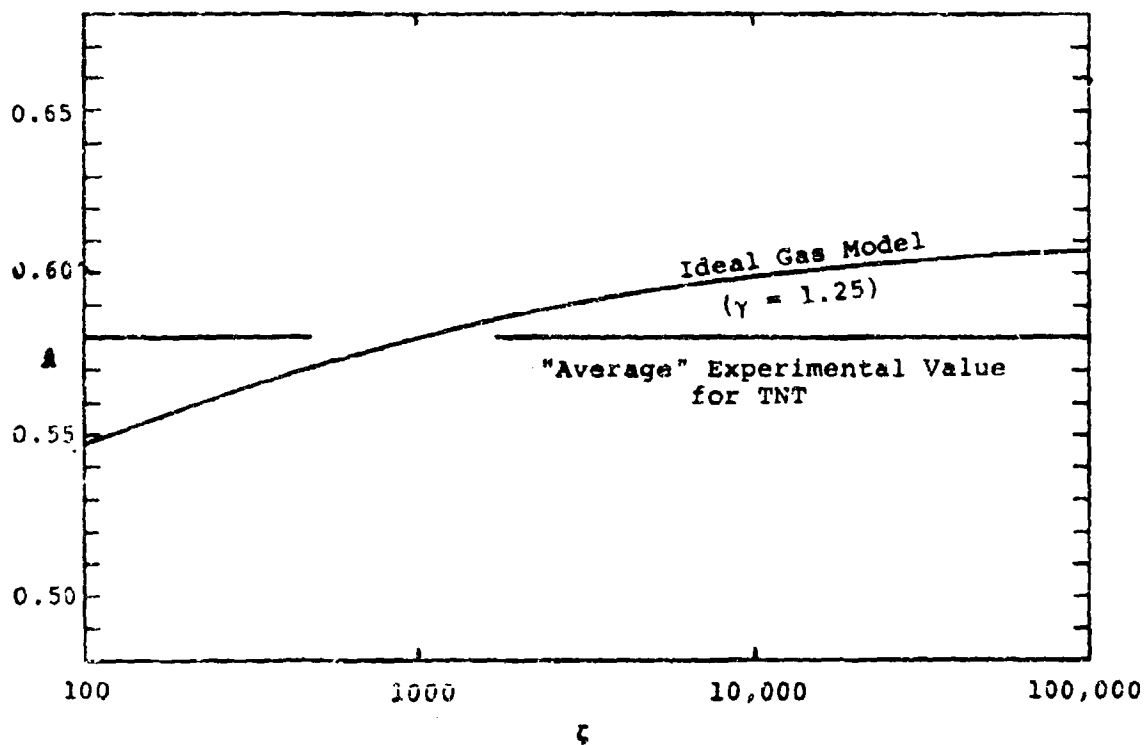
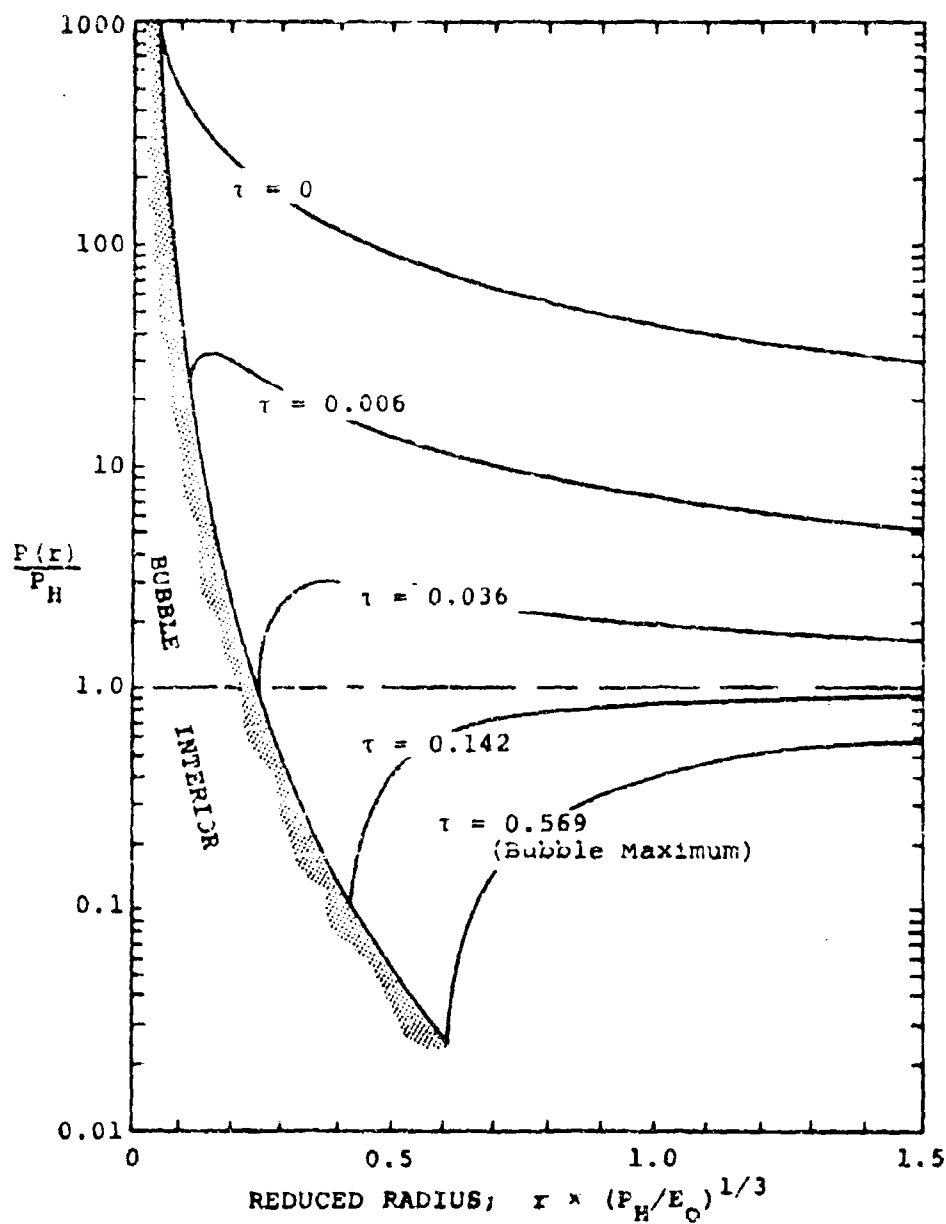


FIGURE 19: COMPARISON OF THE "AVERAGE" EXPERIMENTAL DIMENSIONLESS MAXIMUM BUBBLE RADIUS FOR TNT WITH IDEAL GAS MODEL RESULTS

FIGURE 20: PRESSURE DISTRIBUTION IN THE WATER SURROUNDING  
THE BUBBLE FOR VARIOUS TIMES AFTER BURST  
(Ideal Gas Model:  $\gamma = 4/3$  and  $\zeta = 3000$ )



pressure (which depends on temperature), the water at the bubble boundary will begin to boil, increasing the amount of gas in the bubble, its maximum size, and its period of oscillation. For explosions at normal hydrostatic pressures (greater than one atmosphere), of course, this effect does not occur. If the water is cooled sufficiently, bubble boiling will not occur even for hydrostatic pressures less than one atmosphere. The hydrostatic pressure at which bubble boiling at the maximum would be expected to begin as a function of water temperature is shown in Figure 21. This result should, of course, be taken as approximate; it was derived using the  $\gamma = 4/3$  ideal gas bubble model assuming an initial bubble energy density equal to that of TNT. Actually, Figure 21 is quite conservative; experimental results indicate that significant effects upon bubble behavior do not occur unless hydrostatic pressures are about a factor of four or so smaller than indicated (Snay, 1964). The reason is simply that, although the bubble interior pressure may drop slightly below vapor pressure at the bubble maximum, the amount of water actually vaporized is fairly small due to the very short bubble oscillation period, unless the interior pressure is well below vapor pressure for a substantial part of the oscillation cycle.

A number of experiments using the "vacuum tank technique" were performed at the Naval Radiological Defense Laboratory during the early 1960's using a very high energy density electrically exploded metallic wire as the energy source (Buntzen, 1964; Pritchett, 1966). Such an explosion produces no permanent gases, and therefore the steam bubble generated is similar to that of an underwater nuclear explosion (Buntzen, 1961). Some of these tests occurred in the "danger zone" in which the bubble boiling might be expected; of those which were not, however, the bubble radii and oscillation periods, as measured by high-speed photography, agree fairly well with results predicted using the ideal-gas model. The scatter in this data was, however, considerable; due to the small size of the explosions, bubble periods

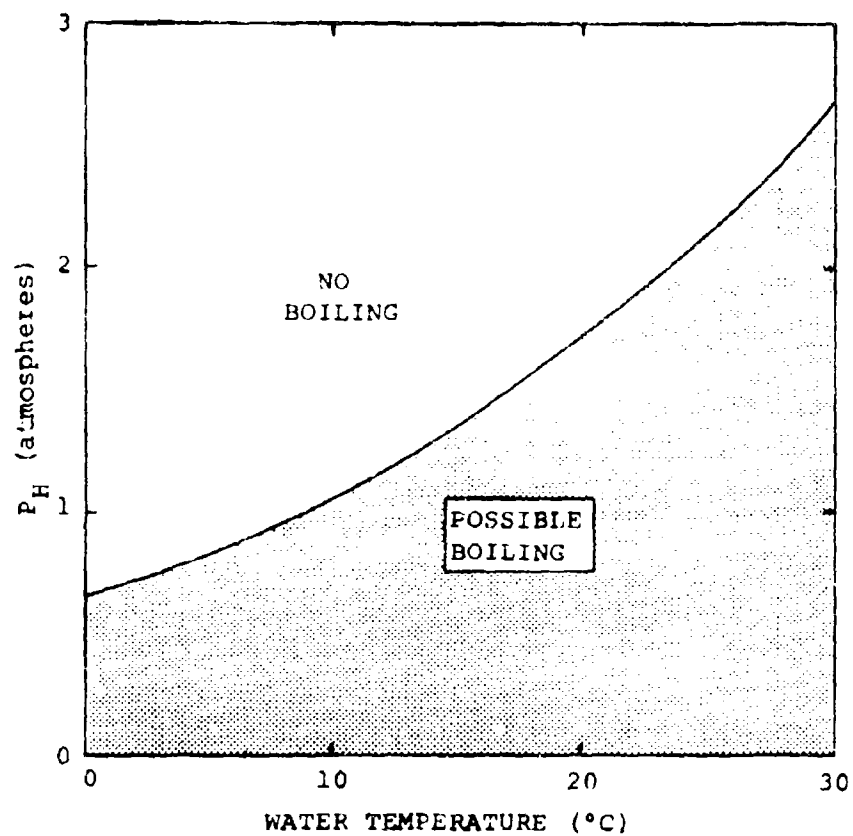


FIGURE 21: CRITICAL AMBIENT HYDROSTATIC PRESSURE BELOW WHICH BUBBLE SURFACE MAY BOIL AT THE BUBBLE MAXIMUM AS A FUNCTION OF WATER TEMPERATURE

were of order a few tens of milliseconds and bubble radii were typically only a few centimeters. Furthermore, the total explosion energy was difficult to reproduce, and could only be determined within 10% or so. None the less, these results also tend to support the ideal-gas model for bubble pulsation.

Other measurements than the maximum radius and bubble period have, of course, been made. The scatter in the measured results is considerable, however, due to the great difficulty in experimentally determining the bubble radius-time relation. The radius-time curve computed using the ideal-gas model falls well within the band of experimental scatter. Measurement of subtle parameters such as  $B$  (the "shape factor") would of course be extremely difficult, and has never been attempted, to the author's knowledge. The "characteristic velocity"  $\mu$ , on the other hand, may be determined if the bubble maximum radius and oscillation period are known. The "average" value which may be derived from the empirical TNT equations (IX-2 and IX-4) is 0.51, which falls in the middle of the range of values derived from the ideal gas model. As has been pointed out by Snay (1960) and others, although the empirical coefficients  $J$  and  $K$  depend upon explosive type, the ratio  $J/K$  is relatively constant at about 2.9 within a few percent, which implies  $\mu = 0.51$ .

As has been seen, the available experimental data, while generally verifying the present results which assume incompressible water, are sufficiently scattered that precise comparisons are simply not possible. In recent years, a few theoretical calculations of one-dimensional bubble motion which include the effect of water compressibility have appeared in the literature. Two of these (Kot, 1964 and Bjork, Kreyenhagen and Wagner, 1969) involved nuclear explosions, and two others, (Phillips and Snay, 1968 and Mader, 1971) represented smaller conventional explosions. Kot considered three cases, all one-kiloton nuclear explosions at burst depths of 91, 305, and 610 meters. The equation of state data used was, regrettably, rather primitive. Bjork, et.

al. considered only one case -- a 10 kiloton nuclear explosion at 1830 meters. Unfortunately, the one-dimensional calculation was terminated at 6.9 microseconds; a relatively poorly-resolved two-dimensional method was used thereafter, but even this calculation ended at 140 milliseconds, so that the bubble never reached its first maximum. Phillips and Snay report the results of five calculations of one-pound TNT explosions at burst depths of 24, 152, 305, 4220 and 6822 meters. Mader's results represent the explosions of half-pound spherical Tetryl charges (a conventional high explosive similar in characteristics to TNT) at hydrostatic pressures corresponding to burst depths of 89, 735, 4610 and 46,600 meters. In reality, of course, the average depth of the ocean is only about 4000 meters and the deepest point is about 11,000 meters (at the bottom of the Mindanao Trench) so Mader's deepest case must be regarded as somewhat hypothetical. The range of depths of interest for underwater explosions generally does not extend below 1000 meters or so.

The maximum bubble radii reported by Kot, Phillips and Snay, and Mader (excluding his deepest case which is off-scale) are shown in dimensionless form as functions of the relative explosion intensity  $\zeta$  in Figure 22. Also shown are the results of the ideal gas model neglecting gas inertial effects for  $\gamma$  ranging from 1.15 to 1.40. The scatter in the "band" of compressible -water computational results is about 10%, but, as can be seen, the overall agreement is fairly good. Similarly, the results of Kot, Phillips and Snay, and Mader for the "characteristic velocity"  $u (= \Lambda/\delta t)$  are compared with the ideal-gas-model results in Figure 23. Also included is the result of an earlier calculation by Keller and Kolodner (1953) in which the water was considered compressible, but the bubble interior was treated as a homogeneous ideal gas with  $\gamma = 1.25$ . Once again, the agreement of the data with the incompressible results appear as good as the agreement between one set of data and another.

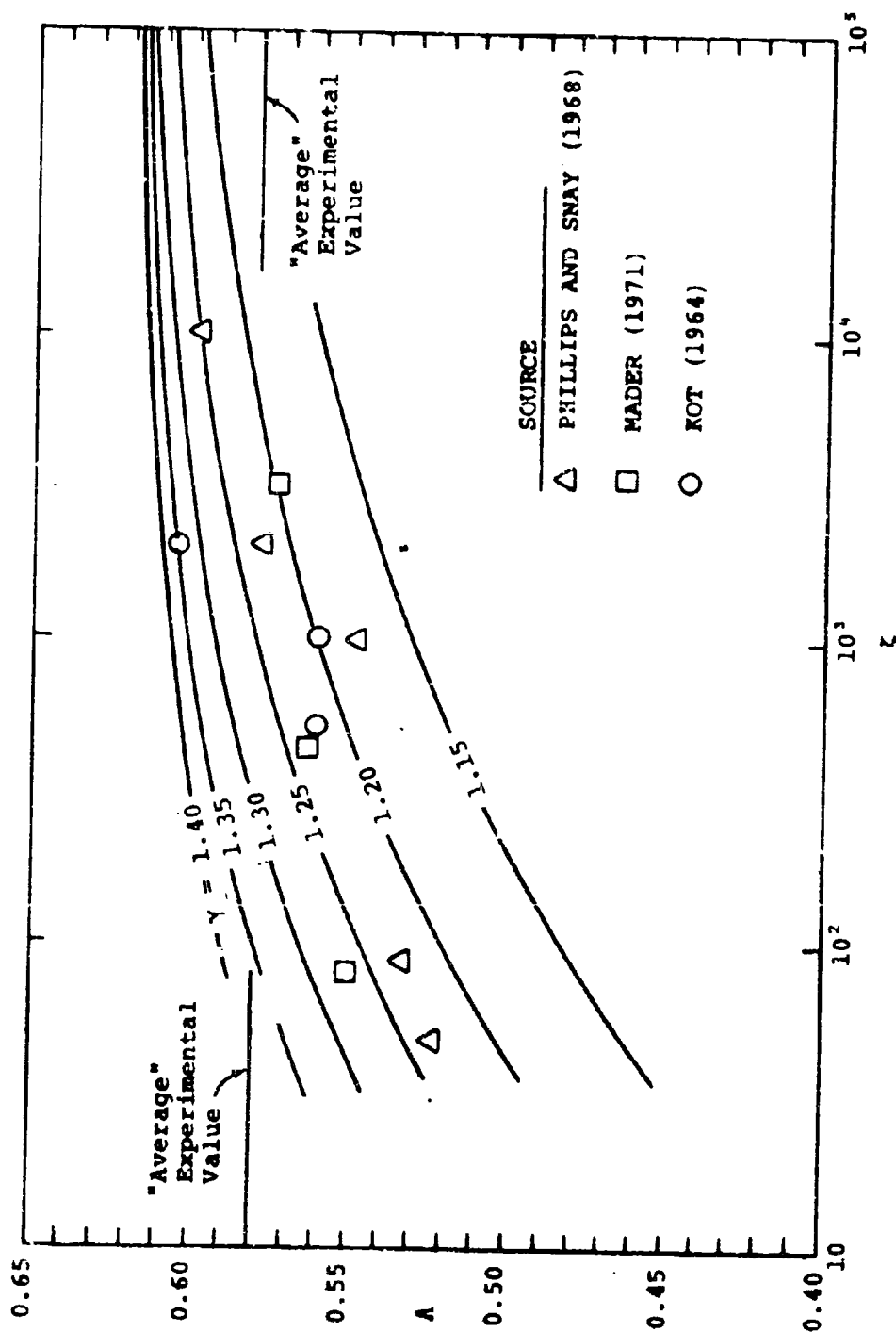


FIGURE 22: COMPARISON OF THE DIMENSIONLESS MAXIMUM BUBBLE RADII ( $A$ ) PREDICTED BY COMPRESSIBLE-WATER CALCULATIONS WITH IDEAL GAS - INCOMPRESSIBLE WATER RESULTS

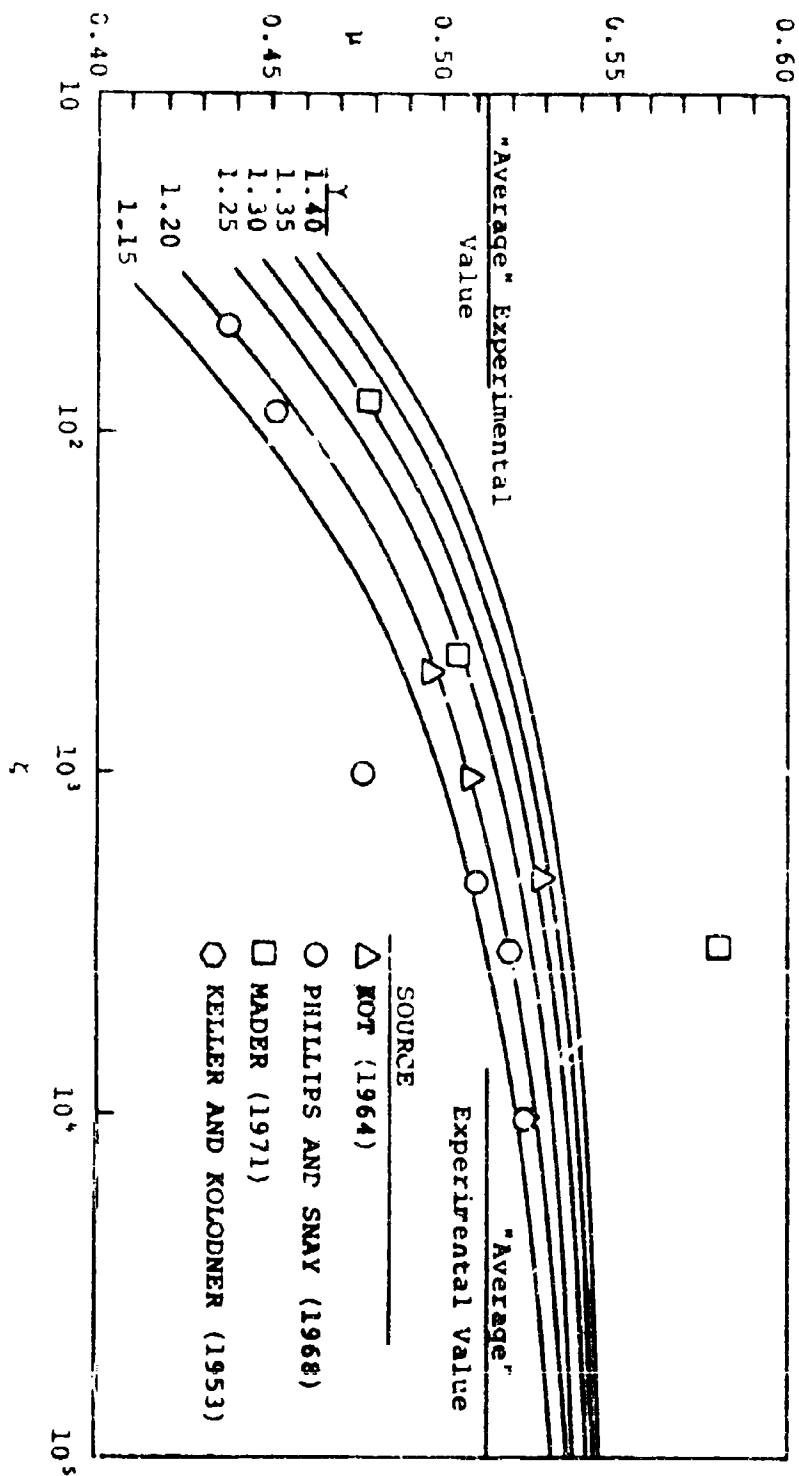


FIGURE 23: COMPARISON OF THE DIMENSIONLESS CHARACTERISTIC VELOCITIES ( $\mu$ ) PREDICTED BY COMPRESSIBLE-WATER CALCULATIONS WITH IDEAL GAS - INCOMPRESSIBLE WATER RESULTS

Although both the experimental measurements discussed earlier and the theoretical results which include the effect of water compressibility tend to agree with the incompressible-water calculations, the scatter in both is sufficiently great that no clear choice based upon these results alone can be made among the various models discussed in the previous sections. The ideal-gas model results agree quite well with experiments and with the compressible-water calculations and, as has been shown, further elaboration of that model (to include gas inertial effects, real-steam behavior, and/or bubble inhomogeneity) alters the results obtained by only fractions of a percent. The deviations of the ideal-gas incompressible-water model results from compressible-water calculations and from experimental measurements are at least as great as the "improvement" that could in principle be obtained by using a more elaborate model for the bubble interior.

It is therefore recommended that the ideal gas model neglecting gas inertial effects be adopted for the purpose of making incompressible-water calculations of bubble motion. The additional complications introduced by using a more complex model are simply not warranted in view of the very slight gain in accuracy, particularly since the assumption of incompressible water itself introduces errors of at least comparable size. As was seen in section VII, for steam bubbles produced by nuclear explosions,  $\gamma = 4/3$  seems to agree best with the real-steam results; for high-explosive calculations, a somewhat lower value (such as 1.25) should probably be used.

X. ACKNOWLEDGEMENTS

The author expresses his appreciation to Dr. S. J. Lukasik, Director of the Advanced Research Projects Agency, for the interest, support, and encouragement which made this work possible, and to Dr. C. Mader of the Los Alamos Scientific Laboratory for a number of helpful technical suggestions.

This research was sponsored by the Advanced Research Projects Agency of the Department of Defense and was monitored by the Office of Naval Research under Contract No. N00014-70-C-0260.

Preceding page blank

XI. REFERENCES

- BJORK, R.L., K.N. FREYENHAGEN and M.H. WAGNER, "Compressible Hydrodynamic Analysis of an Underwater Nuclear Burst," Shock Hydrodynamics, Inc., Naval Radiological Defense Laboratory Report No. NRDL-TRC-69-6, 1969 (Classified).
- BUNTZEN, R.R., "The Use of Exploding Wires in the Study of Small-Scale Underwater Explosions," Exploding Wires, Vol. 2, Plenum Press, New York, 1961.
- BUNTZEN, R.R., "The Underwater Distribution of Explosion Products from a Submerged Exploding Wire," Naval Radiological Defense Laboratory Report No. USNRDL-TR-778, 1964.
- COLE, R.H., Underwater Explosions, Princeton University Press, 1948.
- FRIEDMAN, B., "Theory of Underwater Explosion Bubbles," Institute for Mathematics and Mechanics, New York University Report No. IMM-NYU 166, 1947.
- GAWAIN, T.H. and J.W. PRITCHETT, "A Unified Heuristic Model of Fluid Turbulence," Journal of Computational Physics, Vol. 5, No. 3, 1970.
- KELLER, J.B. and I.I. KOLODNER, "Underwater Explosion Bubbles - I: The Effect of Compressibility of the Water," Institute for Mathematics and Mechanics, New York University Report No. IMM-NYU 191, 1953.
- KOT, C.A., "HYDRA Program -- Theoretical Study of Bubble Behavior in Underwater Explosions," Naval Radiological Defense Laboratory Report No. USNRDL-TR-747, 1964.
- LAMB, H., Hydrodynamics, Cambridge University Press (6th Edition), 1932.
- MADER, C.L. and W.R. GAGE, "FORTRAN SIN -- A One-Dimensional Hydrodynamic Code for Problems Which Include Chemical Reactions, Elastic-Plastic Flow, Spalling, and Phase Transitions," Los Alamos Scientific Laboratory Report No. LA-3720 (1967).
- MADER, C.L., "Compressible Numerical Calculations of Underwater Detonations," Los Alamos Scientific Laboratory Report No. LA-4594, 1971.
- PHILLIPS, D.E. and H.G. SNAY, "The Parameters of Underwater Nuclear Explosion Bubbles," Naval Ordnance Laboratory Report No. NOLTR-68-63, 1968 (Classified).

- PRITCHETT, J.W., "Explosion Product Redistribution Mechanisms for Scaled Migrating Underwater Explosion Bubbles," Naval Radiological Defense Laboratory Report No. USNRDL-TR-1044, 1966.
- PRITCHETT, J.W., "MACYL - A Two-Dimensional Cylindrical Coordinate Incompressible Hydrodynamic Code," Naval Radiological Defense Laboratory Report No. USNRDL-LR-67-97, 1967.
- PRITCHETT, J.W. and J.F. PESTANER, "A Numerical Calculation of the Water Flow Following the WIGWAM Underwater Explosion," Naval Radiological Defense Laboratory Report No. NRDL-TR-69-48, 1969.
- PRITCHETT, J.W., "The MACYL6 Hydrodynamic Code: A Numerical Method for Calculating Incompressible Axisymmetric Time-Dependent Free-Surface Fluid Flows at High Reynolds Number," Information Research Associates, Inc. Report No. IRA-TR-1-70, 1970(a).
- PRITCHETT, J.W., "Incompressible Calculations of Underwater Explosion Phenomena," Proc. Second International Conference on Numerical Methods in Fluid Dynamics, Berkeley, California, 1970(b).
- PRITCHETT, J.W., "The Containment of Underwater Nuclear Explosions: Theoretical Calculations of Deep Burst Hydrodynamics," Information Research Associates, Inc. Report No. IRA-TR-1-71, 1971 (Classified).
- SNAY, H.G. and E.A. CHRISTIAN, "Underwater Explosion Phenomena: The Parameters of a Non-Migrating Bubble Oscillating in an Incompressible Medium," Naval Ordnance Laboratory Report No. NAVORD 2437, 1952.
- SNAY, H.G., "The Behavior and Effects of Underwater Explosion Bubbles," Proc. U.S.N. Bureau of Ordnance Hydroballistic Symposium, Stevens Institute of Technology, New Jersey, 1957 (Classified).
- SNAY, H.G., "The Hydrodynamic Background of the Radiological Effects of Underwater Nuclear Explosions," Proceedings of the Tripartite Symposium on Technical Status of Radiological Defense in the Fleets, Naval Radiological Defense Laboratory Report No. R&L 103, 1960 (Classified).
- SNAY, H.G., "Underwater Explosion Phenomena: The Parameters of Migrating Bubbles," Naval Ordnance Laboratory Report No. NAVORD 4185, 1962.
- SNAY, H.G., "Model Tests and Scaling," Naval Ordnance Laboratory Report No. NOLTR-53-257, 1964.

WELCH, J.E., F.H. HARLOW, J.P. SHANNON and B.J. DALY, "The MAC Method," Los Alamos Scientific Laboratory Report No. LA-3425, 1966.

WILLIS, H.F., "Underwater Explosions: The Time Interval Between Successive Explosions," British Report WA-47-21, 1941.

# APPENDIX A: SYMBOLS AND ABBREVIATIONS

A	instantaneous bubble surface area
B	"shape factor" for bubble oscillation cycle = $\left( \int_0^T R^3 dt \right) / (R_{\max}^3 T)$
C	speed of sound in water
C <sub>det</sub>	detonation wave speed within the explosive
E	total energy per unit mass = $\frac{1}{2} u^2 + H$
E <sub>o</sub>	bubble oscillation energy
E <sub>I</sub>	internal energy of bubble atmosphere
E <sub>I<sub>o</sub></sub>	initial bubble internal energy
E <sub>K</sub>	kinetic energy
E <sub>KG</sub>	kinetic energy of bubble atmosphere
E <sub>KW</sub>	kinetic energy of the water outside the bubble
F <sub>b</sub>	buoyant force
g	acceleration of gravity
H	internal energy per unit mass
I	buoyant momentum
I*	dimensionless buoyant momentum
J	empirical "radius coefficient"
K	empirical "period coefficient"
M	Mach number
P	pressure
P <sub>o</sub>	initial bubble pressure
P <sub>B</sub>	bubble pressure
P <sub>H</sub>	hydrostatic pressure
Q	chemical energy released per unit explosive mass

$r$	radial coordinate
$R$	instantaneous bubble radius
$\dot{R}$	instantaneous bubble interface velocity
$\ddot{R}$	instantaneous bubble interface acceleration
$R_0$	initial bubble radius
$R_{\max}$	maximum bubble radius
$t$	time
$t_R$	reaction time of explosive charge
$T$	bubble oscillation period
$u$	velocity
$U_c$	characteristic velocity for bubble oscillation = $R_{\max}/T$
$V$	bubble volume
$V_0$	initial bubble volume
$W$	work done against external forces
$WT$	charge weight measured in pounds
$Y$	yield; total explosion energy
$z$	axial coordinate variable
$Z$	hydrostatic pressure ( $P_H$ ) measured in feet of water
$\delta\tau$	dimensionless bubble oscillation period
$\gamma$	ideal-gas adiabatic exponent (ratio of specific heats)
$\lambda$	dimensionless instantaneous bubble radius
$\dot{\lambda}$	dimensionless instantaneous bubble interface velocity
$\lambda_0$	dimensionless initial bubble radius
$\Lambda$	dimensionless maximum bubble radius
$\mu$	dimensionless bubble oscillation characteristic velocity ( $\Lambda/\delta\tau$ )

$\pi$	3.14159265...
$\rho$	density
$\rho_E$	explosive packing density; initial bubble density
$\rho_g$	instantaneous bubble interior density
$\rho_w$	water density
$\tau$	dimensionless time
$\zeta$	dimensionless explosion "intensity".